



HAL
open science

The Surface Energy Budget Computed at the Grid-Scale of a Climate Model Challenged by Station Data in West Africa

F. B Diallo, F. Hourdin, C. Rio, A.-K. Traore, L. Mellul, F. Guichard, L. Kergoat

► To cite this version:

F. B Diallo, F. Hourdin, C. Rio, A.-K. Traore, L. Mellul, et al.. The Surface Energy Budget Computed at the Grid-Scale of a Climate Model Challenged by Station Data in West Africa. *Journal of Advances in Modeling Earth Systems*, 2017, 9 (7), pp.2710 - 2738. 10.1002/2017MS001081 . hal-01696565

HAL Id: hal-01696565

<https://hal.sorbonne-universite.fr/hal-01696565>

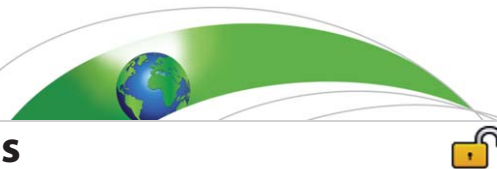
Submitted on 30 Jan 2018

HAL is a multi-disciplinary open access archive for the deposit and dissemination of scientific research documents, whether they are published or not. The documents may come from teaching and research institutions in France or abroad, or from public or private research centers.

L'archive ouverte pluridisciplinaire **HAL**, est destinée au dépôt et à la diffusion de documents scientifiques de niveau recherche, publiés ou non, émanant des établissements d'enseignement et de recherche français ou étrangers, des laboratoires publics ou privés.



Distributed under a Creative Commons Attribution 4.0 International License



RESEARCH ARTICLE

10.1002/2017MS001081

The Surface Energy Budget Computed at the Grid-Scale of a Climate Model Challenged by Station Data in West Africa

F. B. Diallo¹ , F. Hourdin¹, C. Rio², A.-K. Traore¹, L. Mellul¹, F. Guichard², and L. Kergoat³ 

¹Laboratoire de Météorologie Dynamique/IPSL/UPMC Université Paris 06/Sorbonne Universités/CNRS, Paris, France, ²CNRM (UMR 3589 CNRS and Météo-France), Toulouse, France, ³Geosciences Environnement Toulouse (CNRS/IRD/CNES/ Université de Toulouse), Toulouse, France

Key Points:

- Nudging horizontal winds toward reanalysis enables the comparison of a GCM grid cell with station data under same synoptic conditions
- Nudging allows to disentangle biases related to a bad positioning of the WAM from those due to the misrepresentation of physical processes
- Soil thermal inertia, turbulent mixing, surface albedo, aerosols and clouds are all key for the representation of the surface energy budget

Correspondence to:

F. B. Diallo,
bdiallo@lmd.jussieu.fr

Citation:

Diallo, F. B., Hourdin, F., Rio, C., Traore, A.-K., Mellul, L., Guichard, F., & Kergoat, L. (2017). The surface energy budget computed at the grid-scale of a climate model challenged by station data in West Africa. *Journal of Advances in Modeling Earth Systems*, 9, 2710–2738. <https://doi.org/10.1002/2017MS001081>

Received 7 JUN 2017

Accepted 13 OCT 2017

Accepted article online 22 OCT 2017

Published online 23 NOV 2017

Abstract In most state-of-the-art climate models, systematic errors persist in the representation of the rainfall seasonality, near surface air temperature, and surface energy budget over West Africa, even during the dry season. Most biases are related to an incorrect latitudinal position of the monsoon structures. To disentangle the role of the large-scale dynamics from that of the physical processes in these biases, simulations are performed with the LMDZ general circulation model in which the horizontal winds are nudged toward reanalysis. Wind nudging greatly improves the position of the ITCZ as well as the representation of the components of the surface energy budget directly impacted by the water budget and hence facilitates a more systematic analysis of remaining biases associated with the physics in the model. The great potential of wind nudging to compare the energetics of the atmospheric column in climate models at grid cell scale with station observations, even for coarse grid models, is then shown. Despite the improved water advection and rainfall seasonality in the nudged simulations, errors consisting in a cold bias during the dry season over Sahel, an underestimated seasonal variation of surface albedo, and an overestimation of the solar incoming flux remain. The origin of these remaining biases is further investigated by conducting a series of dedicated sensitivity experiments. Results highlight the key role of the soil thermal inertia, the turbulent mixing efficiency, the surface albedo, and the aerosols and clouds radiative effects in the representation of meteorological 2m-variables and surface energy budget.

1. Introduction

General circulation models have difficulties simulating the seasonality of temperature and rainfall in West Africa, a region characterized by a complex climate and where in-situ observations are scattered and challenging to collect. The purpose of this study is to use local observations collected at various sites in West Africa to evaluate and to improve the representation of near-surface temperature and humidity, latent and sensible heat flux, and surface radiation budget simulated by a general circulation model.

The West African climate is characterized by the seasonal migration of the Inter-tropical Convergence Zone (ITCZ) between the coast of the Gulf of Guinea and the Sahara desert. The ITCZ reaches the Sahel in summer resulting in a short rainy season corresponding to the West African monsoon. This complex climate phenomenon, organized at various scales, has been extensively documented during the AMMA (African Monsoon Multidisciplinary Analysis) field campaign (Redelsperger et al., 2006). Land surface thermodynamics and water budget were identified as key components of land-atmosphere interactions, which play a crucial role in the mechanisms involved in the West African monsoon system (Charney, 1975; Eltahir & Gong, 1996; Taylor et al., 2011).

In the 70s and in the 80s, the Sahel experienced a severe drought associated with a warm anomaly in surrounding low-latitude oceans which weakened the in-land excursion of the ITCZ (Giannini et al., 2002). The partial recovery of rainfall since this period has been explained by the end of this temperature anomaly but it was probably also affected by the global warming resulting from the global greenhouse gas increase (Gaetani et al., 2016). According to the IPCC fifth Assessment Report (Stocker et al., 2013), warming may also be significantly stronger in Africa than at the global scale. The warming in Africa may be of the order of 3° C over the coast and 4° C over continental Sahel for a 2° C warming at the global scale. Remarkably clear warming trends have also been documented for the historical period by Guichard et al. (2015). In addition

© 2017. The Authors.

This is an open access article under the terms of the Creative Commons Attribution-NonCommercial-NoDerivs License, which permits use and distribution in any medium, provided the original work is properly cited, the use is non-commercial and no modifications or adaptations are made.

to droughts and warming, West Africa has experienced severe floods in the last decade, in particular in 2007, 2008 and 2009. These extreme phenomena are sometimes attributed to climate change. Beyond the general warming trend, the amplitude of the regional warming and rainfall changes is however highly uncertain. Improving the simulation of past and present climate over West Africa is an ongoing challenge that will lead to a more reliable use of future climate change projections over West Africa.

Because of the constraints related to the computational means, current global climate models (GCMs) use coarse grids with typical grid cell sizes of the order of 100 to 300 km. With such an horizontal resolution, convective and clouds processes are parameterized and not explicitly calculated. Parameterizations of atmosphere surface couplings must also account for the heterogeneities of the surface and soil characteristics. This also applies to regional climate models if their grid is not refined down to a few km or less. Many options exist to parameterize these sub-grid scale processes, which explains for a large part the diversity of climate models. Evaluating the skill of the GCM parameterizations is one main motivation for large international inter-comparison exercises like CMIP (Coupled Model Inter-comparison Project). Analyses focused on the West Africa monsoon (WAM, Roehrig et al., 2013) show that "CMIP5 models have not reached yet a degree of maturity which makes it possible to rely directly on them to anticipate climate changes and their impacts, especially with regards to rainfall". In coupled atmosphere-ocean simulations of the present-day climate, these authors found that the annual cumulated rainfall over a Sahel box (17W-10E; 12.N-20N) varies by a factor of 10 across models. These biases can be partly attributed to warm biases in the simulated sea surface temperature over the Gulf of Guinea, limiting the northward migration of the ITCZ. Even with prescribed sea surface temperature, large biases remain on the position of the zonal jets and ITCZ. Concerning the energy budget, a large deviation is also found between models when comparing temperature and surface fluxes over the Sahel. The deviation reaches typically 7 K on the 2 m temperature, 80 W/m² for the net infrared flux, 60 W/m² for the net solar flux and 40 W/m² for the net radiative budget during the dry season. The causes of these biases are poorly known. During the monsoon period, precipitation plays a key role by controlling the evaporative fraction. Outside of the monsoon period, surface fluxes are more controlled by the radiative impact of water vapor, clouds and aerosols (Guichard et al., 2009; Slingo et al., 2009).

In the present study, we evaluate the simulation of the local meteorological variables and that of the surface energy budget in the LMDZ GCM. The most reliable observations to precisely assess air-surface coupling are ground-based measurements. An unprecedented instrument deployment during AMMA helped documenting surface fluxes and near surface meteorological variables along a latitude transect in West Africa (Lebel et al., 2009) as well as the mesoscale variability due to land use and land cover (Lohou et al., 2014; Ramier et al., 2009; Timouk et al., 2009). One motivation of the present study is to estimate how a direct comparison of the model outputs with AMMA site measurements can be used to improve the understanding and modeling of the surface-atmosphere coupling. This motivation leads to methodological questions. The first question concerns the representativeness of point stations observations when comparing them with the grid cell of a model, which aims at representing the average of meteorological variables on scales of typically 200 × 200 km². The second issue is related to the chaos in the meteorological system. Even if initialized with observations, the day-to-day simulation of the meteorology would rapidly diverge from the real one. Because of this well-known issue of the climate models, the comparison with observations is usually done in terms of statistics computed on 10-year simulations for instance. By doing this, a large part of the information that the multi-variate station data contains would be lost.

This issue can be avoided by forcing the simulated day-to-day evolution of the meteorology to follow the real one by applying so-called nudging techniques to the large-scale dynamics. In practice nudging consists in relaxing the horizontal winds of the model toward those of the analyzes or reanalyzes produced by numerical weather forecast centers with a typical time constant of several hours. The potential of these nudging techniques has already been demonstrated by comparing LMDZ simulations with in situ observations at SIRTA (an observation site located in the mid-latitudes in the Paris area) in studies focusing on the boundary layer physics and the surface coupling (Cheruy et al., 2013; Coindreau et al., 2007). Nudging made it possible to compare model results with local observations on a day-to-day basis, while the seasonality was not much affected by nudging. In this case, it appeared that representativeness was not an issue once it had been checked that the surface local properties for hydrology at the considered grid cell were consistent with that of the observation site.

Here we investigate to which degree this methodology can also be applied in West Africa. In West Africa, an additional methodological question arises (Hourdin et al., 2010; Roehrig et al., 2013): the climate is strongly contrasted in latitude, following the latitudinal distribution of the annual rainfall. Therefore the behavior of local processes strongly depends on this annual rainfall. When considering a climate model with significant rainfall biases (as is generally the case), a direct comparison to site observations will mainly reflect the fact that simulations and observations do not concern the same climatic regime. One way to avoid the above mentioned difficulty would be to compare model outputs with site observations not at a given location but for a similar annual rainfall. For a model with a rainfall deficit over Sahel, this could be done by artificially shifting the location of the point used to extract the simulated variables toward a lower latitude (the rainfall increasing from North to South over Sahel). However, by doing so, one would face other issues, the sunlight and local surface conditions being in this case different between simulation and observation. Here we show that nudging, in addition to the above-mentioned properties, allows the simulated rainfall seasonal cycle to be closer to the observed one, making a direct comparison with observations relevant for other variables.

The methodology used here consists in imposing the model dynamics without constraining the physical parameterizations behavior in order to address the following questions: 1) what is the potential of the nudging technique for the model evaluation and model improvement using site observations in the African monsoon region? 2) To which degree of accuracy can the nudged model reproduce the seasonality, and the intra-seasonal and inter-site variability of the observed surface energy budget? 3) What are the key elements of the physical model that matter in the representation of the surface energy budget?

The tools and method to compare the GCM grid cell with in-situ observations are presented in section 2 and 3 for two versions (LMDZ-5A and LMDZ-5B) of the LMDZ climate model that were used for the last CMIP5 exercise (Hourdin et al., 2013a). The 5B version was based on a deep rewriting of the physical parameterizations of turbulence, convection and clouds. This new version, which in particular much better represents boundary layer convection and clouds as well as the diurnal cycle of deep convection over continents (Rio et al., 2013), was used as a basis for the CMIP6 version under development. Section 4 is dedicated to the documentation and discussion of biases related to the energy budget in this 5B version, both with and without nudging. This helps identifying the part of the biases that are a consequence of the biases in the large-scale dynamics from those caused by errors in parameterizations. In section 5, we explore ways for improvement based on specific sensitivity experiments performed with the LMDZ-5B version of the model.

2. Model and Observational Setup

2.1. Model

The LMDZ model used here is a General Circulation Model (GCM) developed since the 80s (Sadourny & Laval, 1984) at Laboratoire de Météorologie Dynamique (LMD). The “Z” in “LMDZ” stands for “zoom” and it means that the grid can be refined on a specific region (Idelkadi et al., 2005). The model is composed of two parts: 1) a dynamical core in which the three dimensional primitive equations are discretized on a longitude-latitude horizontal grid, and 2) a physical part in which the vertical transfers of heat, moisture and momentum associated with physical parameterizations are computed. The physical part consists of independent vertical columns that exchange information horizontally via the dynamical core, which updates the model state variables, i.e., average pressure, temperature, winds and tracers in the various grid cells. The vertical discretization is based on a so-called hybrid $\sigma-P$ coordinate.

We focus here on the two model versions with 39 vertical levels used for the previous CMIP5 exercise: the LMDZ5A version (Hourdin et al., 2013b) called “OLD physics” and the LMDZ5B version called “STD physics” in the following.

In the OLD physics, the radiative transfer is calculated using broadband spectral models in the visible (Foucart & Bonnel, 1980) and thermal infrared (Morcrette, 1991). Seasonally-varying ozone and aerosols are prescribed for the radiative computations, using prescribed climatologies as done for the CMIP5 experiments with the IPSL-CM5 model (Dufresne et al., 2013). The turbulence in the boundary layer is represented by a turbulent diffusion scheme (Deardorff, 1970). The parameterization of deep convection is based on the mass flux scheme of Emanuel and Zivkovic-Rothman (1999). The cloud fraction associated with convection is calculated from the condensed water computed by the convection scheme (Bony & Emanuel, 2001). Large-scale clouds are predicted from the total amount of water in the model grid-cell and from the

moisture at saturation by using a subgrid-scale distribution of the total water with an imposed width. The effect of subgrid-scale orography is accounted for using the parameterizations of Lott and Miller (1997).

The STD or 5B version is based on a 15-year research at LMD on the parameterization of the convective boundary layer, clouds and deep convection (Hourdin et al., 2013a).

The first major improvement concerns the representation of the convective boundary layer for which a specific mass-flux parameterization of the organized thermal cells or rolls was developed. Combined with an eddy diffusion parameterization based on a prognostic equation for turbulent kinetic energy (Yamada, 1983), the so-called thermal plume model allows up-gradient transport of potential temperature in the convective atmosphere (Hourdin et al., 2002) and a much better representation of the vertical transport of trace species (Locatelli et al., 2015) and horizontal momentum (Hourdin et al., 2017). Over the Sahel, this new parameterization was shown to well reproduce the morning maximum of near surface wind, associated with the downward transport of momentum stored in the low-level nocturnal jet. This wind maximum is responsible for probably half of the dust emission in that region in the dry season. The thermal plume model was extended to the representation of the vertical transport within cloudy convective boundary layers (Rio & Hourdin, 2008; Rio et al., 2010). A specific cloud scheme was then developed to compute the associated cumulus cloud cover, based on a bi-Gaussian subgrid scale distribution of the saturation deficit, which moments are directly computed from thermal plume properties (Jam et al., 2013).

The second major improvement of the 5B version concerns the representation of deep convection. It includes a parameterization of the cold pools that are created below storms by re-evaporation of convective rainfall. It is the first time that such a scheme is introduced in a climate model (Grandpeix et al., 2010). Deep convection is controlled by sub-cloud processes (Rio et al., 2013): it is triggered when the lifting energy provided either by the thermal plume model or the cold pool parameterization overcomes the convective inhibition and its intensity is deduced from the associated lifting power available above the inhibition. These new formulations for convective closure and triggering allow in particular to delay the onset of continental precipitation and its maximum from midday to late-afternoon (Rio et al., 2009), correcting a long-standing bias of large-scale models.

The LMDZ5B version of the model is at the basis of the new LMDZ6 version under development for CMIP6. The present study is largely motivated by the will to evaluate and improve this new physical package over West Africa.

Both versions of LMDZ are coupled to the land surface model ORCHIDEE (Organising Carbon and Hydrology In Dynamic Ecosystems, Krinner et al., 2005) based on the SECHIBA scheme for the hydrological exchange between the Earth's surface and the atmosphere (Schematization of the exchanges of water at the Interface between the Biosphere and the atmosphere; Ducharne and Laval, 2000) and the STOMATE model (Saclay Toulouse Orsay Model for the Analysis of Terrestrial Ecosystems) for vegetation growth.

2.2. Simulations Setup

The simulations setup follows the AMIP protocol (Atmospheric Model Intercomparison Project) in which models are integrated in time from initial conditions and a seasonally varying sea surface temperature is imposed. Simulations are run on a regular grid with a resolution of 300 km in longitude and 200 km in latitude. Two configurations are used. The first configuration called "FREE" hereafter consists in a classical AMIP simulation run from 1 January 1979 to 31 December 2006. In the second configuration, called "NUDG" hereafter, winds are nudged (or relaxed) toward meteorological reanalysis in order to constrain the large-scale dynamics using the following expression:

$$\frac{\partial X}{\partial t} = M(X) + \frac{X^a - X}{\tau} \quad (1)$$

where X represents a model state variable, M is the computation of the time derivatives of this state variable by the model, X^a is the equivalent field for the reanalyses, and τ is the relaxation time constant. The only variables nudged here are the horizontal wind components, the aim being to assess the representation of the thermodynamics and of the water and energy budget at the surface for an imposed large-scale circulation. The winds are taken from the ERA-Interim reanalyses (European Reanalysis for the global Atmosphere, Dee et al., 2011). They are interpolated linearly on the LMDZ horizontal grid, on the 39 vertical layers and in

Table 1
Description of the Automatic Weather Station Sites

Name	Country	Coord.	Ecosystem	Annual rainfall (mm)	Reference
Bamba	Mali	1.4° W 17.1° N	Semi-desert steppe: scattered perennial and annual grasses	150	Timouk et al. (2009)
Agoufou	Mali	1.5° W 15.3° N	Sahelian grassland annual grasses, scattered trees (3%)	350	Timouk et al. (2009) Guichard et al. (2009)
Wankama-millet	Niger	2.6° E 13.6° N	Millet crop	560	Ramier et al. (2009)
Wankama-fallow	Niger	2.6° E 13.6° N	Fallow: annual grasses and shrubs.	560	Ramier et al. (2009)
Nalohou	Benin	1.6° E 9.7° N	Fallow within crops mosaic	1190	Mamadou et al. (2014)
Bira	Benin	1.6° E 9.7° N	Savanna	1190	Mamadou et al. (2014)

time between the 6 hours interval at which they are available for nudging. The relaxation time constant is fixed to $\tau = 3$ hours. From previous experience, it is known that a time constant of several (3 to 12) hours is short enough to constrain the large-scale circulation and long enough for the physical parameterizations to operate (for wind nudging at least). For this study, it was checked that the results are only weakly affected by increasing the time constant up to 12 hours (an illustration is shown at the end of Section 3.1).

2.3. Observations

The station network used here has been designed to document the latitude transect from 12° to 17.1° N and to allow comparison with models at local and mesoscale resolution. The accuracy of the different fluxes has been investigated (Guichard et al., 2009; Mamadou et al., 2014; Ramier et al., 2009; Settle et al., 2008; Timouk et al., 2009) showing that differences of 10 W m^{-2} at the daily timescale should not be considered to be significant for the radiation fluxes, as opposed to differences of tens of W m^{-2} . Uncertainty on turbulent fluxes typically ranges from 5% to 15%, affecting mainly the latent heat flux. This data has been used in a number of Land Surface Model evaluation studies in the framework of ALMIP-2 (Grippa et al., 2016) and other studies (Bateni et al., 2014; Leauthaud et al., 2017; Lohou et al., 2014; Roehrig et al., 2013). This is the first time that it is used to evaluate and analyze the physics of a GCM over the AMMA transect. The main characteristics of the observation sites are summarized in Table 1 and more details on the sites and data can be found on the AMMA-CATCH database (Lebel et al., 2009, <http://www.amma-catch.org>). Automatic weather stations have been recording 2m air temperature and humidity at a 15 minutes or 30 minutes time-step (HMP45C or WXT510, Vaisala), and rainfall with automated rain gauges. The four components of the radiation budget were acquired using CNR1 (Kipp & Zonen). Turbulent fluxes were measured with eddy covariance stations (LiCor7500 gas analyzer, Cs-3 sonic anemometer). The stations form clusters in northern Benin (Nalohou and Bira; Mamadou et al., 2014), southwestern Niger (Ramier et al., 2009) and northern Mali (Guichard et al., 2009; Timouk et al., 2009) and are completed by a single northernmost station in Bamba (Timouk et al., 2009). The main landscape units have been instrumented (i.e., fallow and millet in Niger and crop and savanna in Benin) to document the variability of upward turbulent and radiative fluxes, which are known to depend on surface characteristics, aiming at bracketing mesoscale average fluxes in Niger and Benin. The Agoufou station in Mali is set up on a typical Sahelian grassland. It has been shown to be close to the mesoscale average in terms of surface fluxes (Timouk et al., 2009). The landscape around the northernmost Bamba station is fairly homogeneous. Here, data from these six stations, from north to south Bamba, Agoufou, Wankama-millet, Wankama-fallow, Nalohou and Bira are used. Their main characteristics are presented in Table 1.

We focus on the year 2006, year of the AMMA Special Observing Period (Janicot et al., 2008).

3. Assessment of the Nudging Methodology

In this section, we show how the wind nudging corrects a strong dry bias over the Sahel in the LMDZ model. The comparison of the OLD and STD versions illustrates the robustness of the approach, but also

shows that the nudging technique still lets enough freedom for the model physics to influence the model behavior.

3.1. Impact of Nudging on Moisture Advection and Precipitation

As illustrated in Figure 1a, the STD version of the LMDZ GCM produces a deficit of precipitation in the FREE simulations over the central and northern Sahel in comparison with GPCP (Global Precipitation Climatology Project) during the summer monsoon. In the model, the 1 mm/d contour for the mean July–August–September rainfall remains south of 15° N while it should be located about 3° or 300km further north. This results in a bias of about 2 mm/d (colored shadings on the same map). The zonal wind biases averaged between 10° W and 10° E (color in Figure 1b) display a dipole structure in the middle and upper atmosphere. This dipole corresponds to a southward shift of the African Easterly Jet (AEJ) center located between 600 hPa and 700 hPa and close to 12° N in ERA-Interim. The biases in both rainfall and zonal wind thus indicate that the monsoon system is located too far south in the FREE simulations. Applying the nudging to horizontal winds clearly improves the representation of the monsoon circulation, as seen from the reduction of the mean zonal wind bias (Figure 1d) but it also improves the spatial distribution of rain over Sahel (see

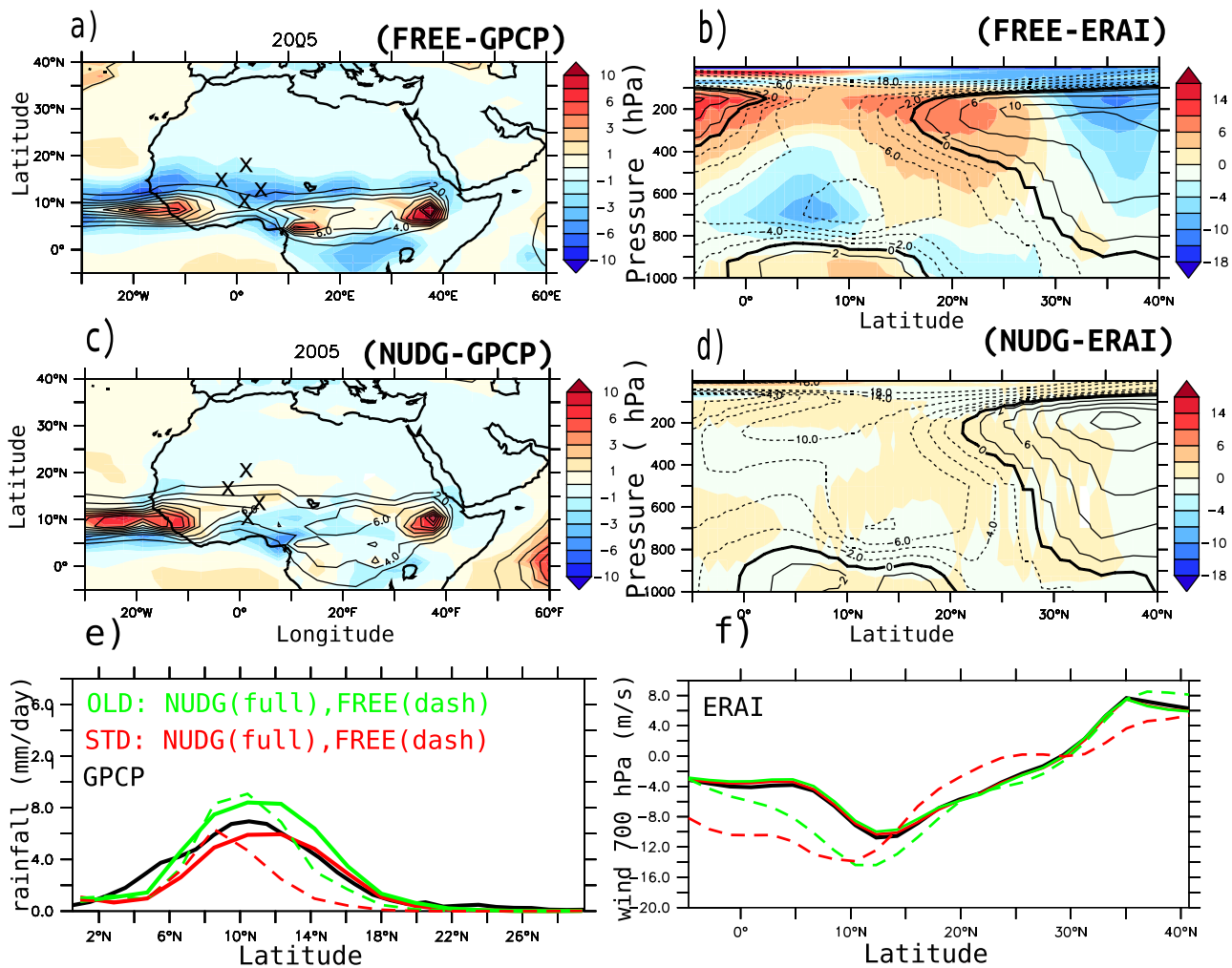


Figure 1. (a and c) Biases (colors) in the simulated rainfall (in mm/d) and (b and d) mean zonal wind between 10° W and 10° E (in m/s) compared with GPCP observations and ERA-Interim reanalysis respectively. The model values (contour lines) and observations are averaged over the period July–August–September (JAS). The comparison is shown both for the FREE (Figures 1a and 1b) and NUDG simulations (Figures 1c and 1d). The black crosses on the rainfall maps represent the Bamba, Agoufou, Wankama and Nalohou sites. The panels e and f represent the latitudinal distribution of rainfall and mean zonal wind at 700hPa averaged between 10° W and 10° E. The black curve represents the reference (GPCP observations in e, ERA-Interim reanalysis). The green and red curves represent respectively the OLD and STD versions of the model in free (dash) and nudged mode (full line).

Figure 1c). The impact of nudging on the latitudinal distribution of rainfall and zonal wind at 700hPa averaged between 10° W and 10° E is further illustrated in Figure 1e and f for the two versions of the model physics. While winds converge between these two nudged versions of the model, there are still differences in the simulated distribution of surface rainfall, the amount of rainfall being less in the STD than in the OLD version of the model. So, for both physics, nudging produces a northward shift of the ITCZ, in better agreement with observations, but on average, rainfall is higher in the OLD than in the STD physics, both with and without nudging. Those differences can be attributed to differences in model physics. In particular, mixing between convective plumes and their environment has been revisited between the OLD and STD versions of the model (Grandpeix et al., 2004), making convection more sensitive to tropospheric humidity, which tends to reduce precipitation in semi-arid regions such as the Sahel.

The effect of nudging on the rainfall distribution is illustrated at the continental scale in Figure 1 by comparing simulations and GPCP satellite observations. This result holds when considering local in-situ observations as illustrated in Figures 2c and 2d for the Bamba station. Nudging, with both the STD and the OLD physics, leads to a better representation of the cumulated distribution of rainfall in comparison to the FREE simulations.

Again, we note that the simulated precipitation differs between the OLD and STD physics in nudged mode: it begins later in the season with the STD than with the OLD physics, in better agreement with observations, while the cumulated rainfall is larger than observed with the OLD physics and lower than observed with the STD physics.

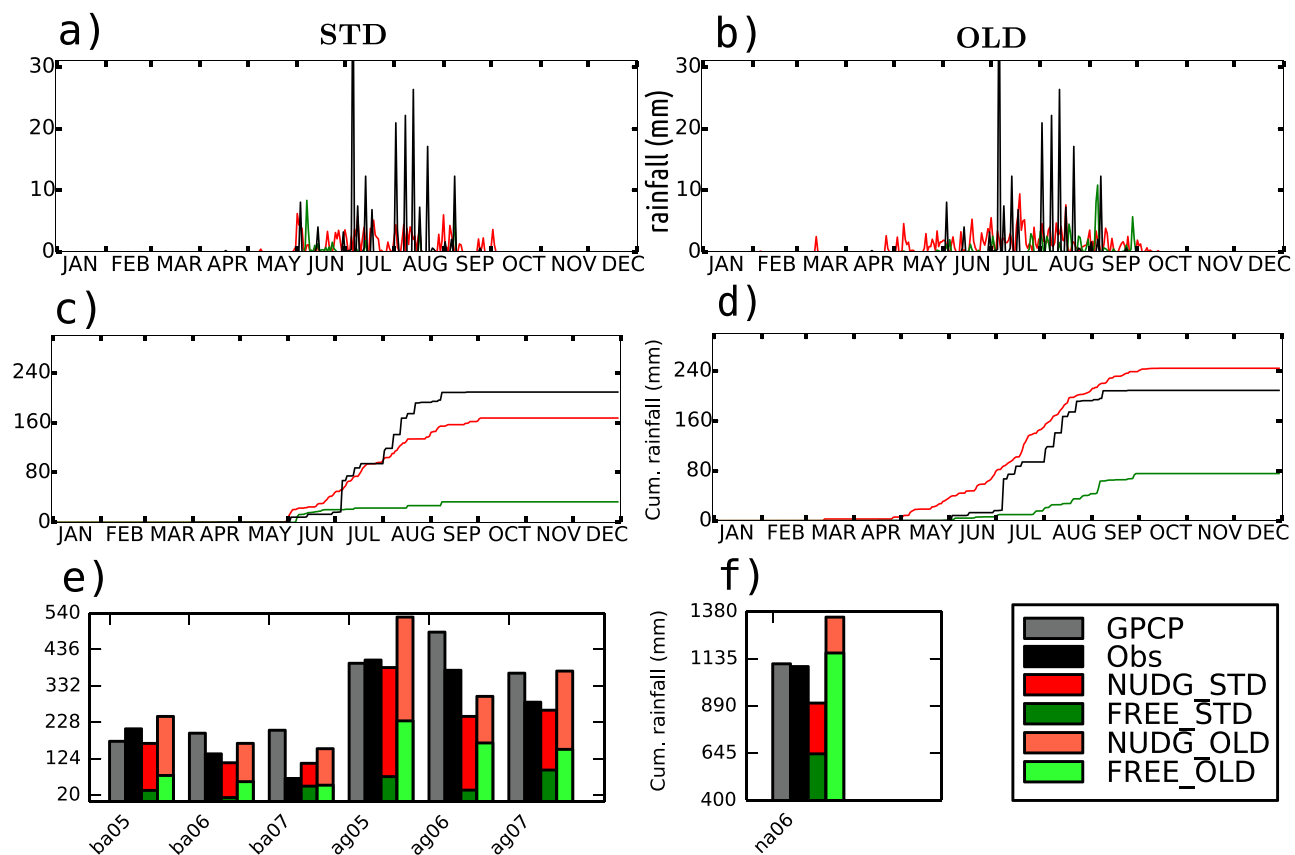


Figure 2. (a and b) Time series of the daily and (c and d) cumulated rainfall, in mm/d, for year 2005 at the Bamba station (1.4E, 17.1N). The black curve represents the in situ observations, the red one represents the NUDG simulation and the green one represents the FREE simulation. Panels a and c correspond to the STD physics and Figures 2b and 2d corresponds to the OLD physics. The bar charts on Figures 2e and 2f show the annual cumulated rainfall at Bamba and Agoufou (1.5 W, 15.3N) stations for years 2005–2007, and at Nalohou (1.6E, 9.7N) in 2006. The in situ (black) and satellite (grey) observations are compared with the results of the STD (dark colors) and OLD physics (light colors). The results of the NUDG simulations correspond to the total bar (green + red) and the result of the FREE simulations correspond to the green bars.

Figures 2e and 2f show the annual cumulated rainfall from 2005 to 2007 over the Sahelian stations of Bamba and Agoufou and at the Sudanian station of Nalohou in 2006. The impact of nudging on physics is similar for the various stations and years: the cumulated rainfall is larger and in better agreement with observations when nudging is applied (except for the Nalohou station with OLD physics), and somewhat larger with the OLD than with the STD physics.

Satellite GPCP observations are shown as well in panels e and f. The comparison with the in-situ observations gives an idea of the observational uncertainty which can come from instrumental errors, retrieval algorithms for GPCP or representativeness for in-situ measurements. The difference between the two sets of observations, which varies spatially and temporally, is generally small enough to assess the effect of nudging and demonstrate that the nudged simulations perform better than the free ones. Yet, this uncertainty is too large to decide which physics performs better. Finally, when considering the daily evolution of precipitation at the Bamba station (see Figures 2a and 2b), the rainfall events in the NUDG simulations with both physics are less intense and sporadic than observed. The same is true at the other stations (not shown).

The effect of nudging on the rainfall seasonality is closely related to the control of moisture advection, which is much better represented in the NUDG configuration as illustrated in the first column of Figure 3 that shows the seasonal evolution of the 2 m specific humidity q_{2m} at the various stations from North to South. The lower graphic also shows the time series at Bira and Nalohou, two Sudanian sites close to each other and characterized by different land uses (cf. Table 1). They are located in the same model grid cell, so that their differences illustrate representativeness errors. The time series of q_{2m} at these two stations almost

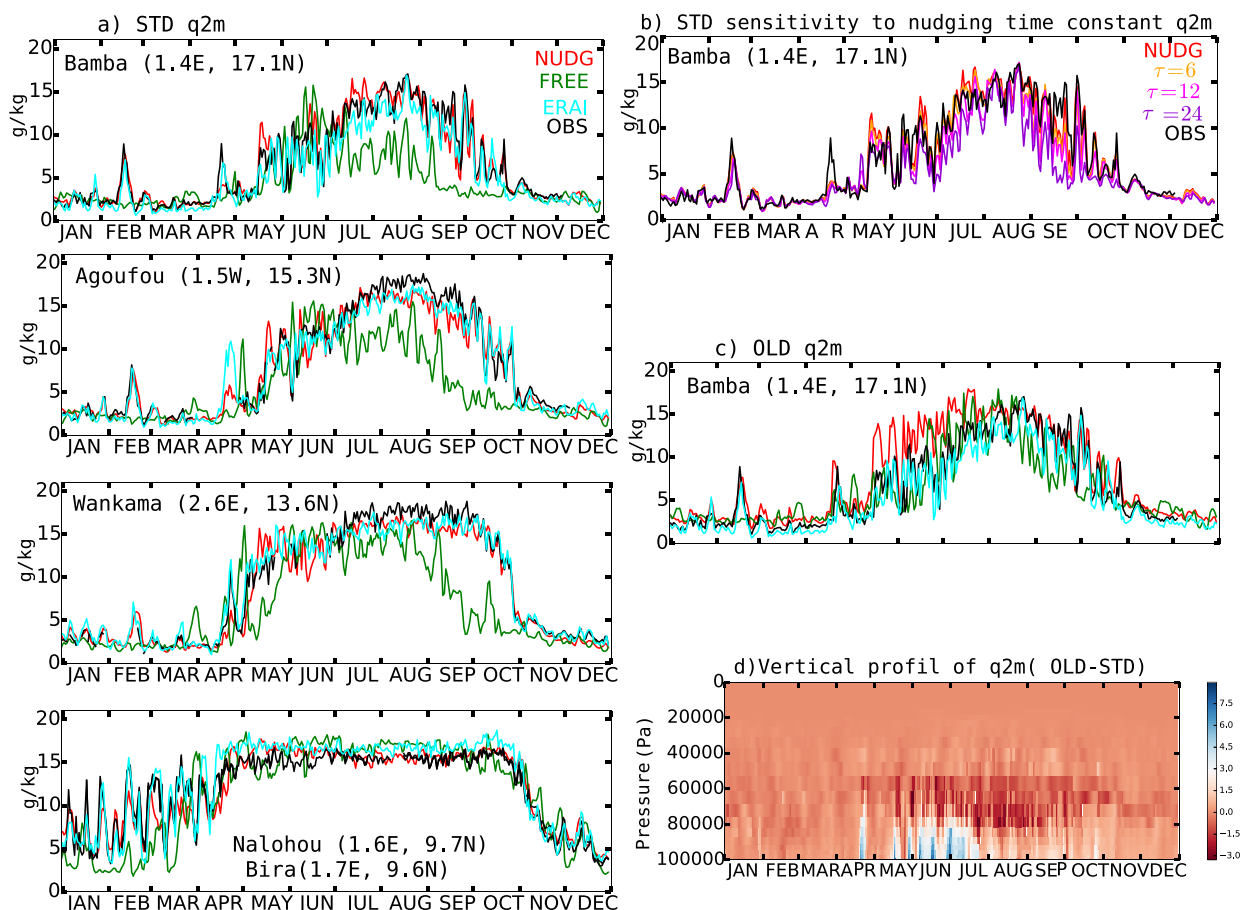


Figure 3. Time series of the daily 2 m specific humidity (in g/kg) for year 2006 at the Bamba, Agoufou, Wankama, and at the Bira and Nalohou stations. Local observations (black) and ERA-Interim (cyan) values are compared with the NUDG (red) and FREE (green) simulations with the STD physics (a, left column). For the Bamba station, results are shown as well for various nudging time constants (b) and for the old physics (c). The bottom-right panel (d) shows the time series of the vertical profile of the difference of the specific humidity between the OLD and STD simulations at Bamba.

overlap. The seasonal evolution of q_{2m} at the Sahelian stations (Bamba, Agoufou and Wankama) is driven by the Harmatthan wind that brings dry air from the Sahara during the dry season and by the monsoon flow that transports moisture over land from the Atlantic ocean, and in particular from the Gulf of Guinea between May and October. Figure 3 highlights the marked climate distinction between the Sahel and the Sudanian zone both in the observations and in the simulations. Over the Sahel, the air is very dry in winter and until May, with specific humidity of the order of 2 g.kg^{-1} and occasional incursions of moist air. In the Sudanian zone, the monsoon lasts longer than over Sahel and is associated with more variability of q_{2m} and a moister winter. The activation of nudging (red curve in Figure 3) leads to a better agreement of the simulated seasonality of q_{2m} with observations. With nudging, the monsoon flow penetrates further north (not shown), which leads to a corrected strong dry bias noted in summer over the Sahel in the FREE simulations. The better representation of the moisture advection in turn leads to an improved simulated monsoon rainfall in this area. Nudging also improves the representation of the day-to-day variability of the 2 m specific humidity during the dry season. While nudging is applied to winds only, the variability of 2 m specific humidity is as well captured by the model as it is by the ERA-Interim reanalysis. In particular in the Sudanian zone, the humidity rate during the rainy season is closer to observations in the NUDG simulations than in the reanalysis.

For the Bamba station, we present in Figure 3b the time evolution of q_{2m} for time constants varying from $\tau = 3$ to $\tau = 24$ h. During the dry season, the curves are almost superimposed for the various time constants. It appears that even a time constant of 24 h is short enough to guarantee a good phasing of the simulated day-to-day evolution with observations. During the rainy season, as could be expected from the comparison of the FREE and NUDG simulations, the atmosphere is drier for a longer time constant. However, even for a time constant of 24 h, the humidity is closer to observation than in the FREE simulation.

3.2. Compared Impact of Nudging and Physical Parameterizations on Simulated Water Vapor

Even when the winds are nudged, the OLD version of the model departs from observed humidity as illustrated at the Bamba station in Figure 3b. The near surface air is often wetter than observed, especially from May to July, while it is drier and in better agreement with observations in the STD version. To understand this result, the vertical distribution of specific humidity is compared between the NUDG OLD and NUDG STD simulations (see Figure 3d). The middle troposphere is moister and the near surface drier in the STD than in the OLD version. This is a direct consequence of the representation of non-local vertical convective transport within the boundary layer by the thermal plume parameterization at play in the STD version. This thermal plume parameterization strengthens the vertical transport of moist air upward from the surface and of dry air downward from the free troposphere. A similar behavior is observed at the other stations (not shown). This attribution of a model bias to a particular parameterization would have been more difficult in a free simulation, in which the modification of humidity could either come from physical parameterizations or from advection by large-scale dynamics, itself coupled to physics parameterizations. Indeed, the seasonal cycle of q_{2m} is better simulated with the OLD than with STD physics in the FREE simulations because of the compensation of errors between underestimated meridional transport and underestimated vertical mixing.

As shown previously, the physics also impacts the cumulated rainfall, which is always larger in the OLD than in the STD version. This is due to changes in the convection scheme but also to the coupling between the boundary layer and convection, or to surface recycling of water on its way from the Gulf of Guinea. Interestingly, this sensitivity is very similar in the free and nudged simulations.

To summarize, the nudging technique allows for the correction of the main model biases associated with the position and timing of the key features of the monsoon system. With nudging, the model better captures the total monsoon rainfall and its seasonality, as well as the annual cycle and synoptic and intra-seasonal variations of near surface specific humidity, both in the Sahelian and the Sudanese regimes. Both versions of the model still differ however, due for example to the introduction of the thermal plume model in the STD physics that improves the representation of near surface specific humidity throughout the West African region and to the modification of convective mixing that inhibits convection in dry regions. Nudging allows to make comparison with in-situ measurements relevant while letting enough freedom to the physical parameterizations to play a role in the model behavior.

4. Characterization of Energy Biases

The energy transfers between the surface and the atmosphere occur either in the form of radiation received from the sun in the visible, ultra-violet and near infra-red spectral domains, and emitted by the atmosphere and surface in the thermal infra-red, or in the form of sensible (H) and latent (LE) turbulent heat fluxes. The flux continuity at the surface reads $G=R_{net}+H+LE$ where R_{net} is the surface net radiation. The ground heat flux G is comparable in intensity to the other fluxes at sub-diurnal scales but its contribution essentially cancels at seasonal time scales.

In this section, the sources of biases in the surface energy budget are identified and characterized. The aim is to assess the realism of the STD physics compared to observations with a focus on the representation of local atmospheric process and surface couplings. As already mentioned, the STD version is favored in this analysis because it constitutes a significant step forward in the physical content and realism of the representation of the vertical transport in the convective boundary layer and of the diurnal cycle of boundary-layer cumulus and storms. Results for the OLD physics are also shown when they help interpreting the origin of a given bias.

For the STD version, both the FREE and NUDG simulations are discussed. A good simulation in the FREE mode is of course the ultimate goal of the work on model improvement within which this paper takes place. As already discussed, the NUDG simulation allows a day-by-day comparison with observations. It also prevents from having a close agreement with observation due to compensating errors between the large-scale dynamics and the parameterized physics. The comparison of the FREE and NUDG simulations allows to identify which part of the energy biases in the FREE mode is related to the erroneous position of the dynamical structure of the monsoon.

4.1. Surface Radiation and Energy Balance

The impact of nudging on the latent and sensible heat fluxes simulated by the model is illustrated in Figure 4 for Wankama where data is available for 2006. In the observations, the latent heat release is quasi null before the rainy season starts, as expected. The latent heat release increases after rain starts and it is higher from July to September, with values reaching 120 W/m^2 . After the rainy season, the latent heat release decreases gradually. The evaporation rate is much lower on average and very intermittent in summer when nudging is deactivated (FREE versus NUDG simulations). Nudging leads to increased rain in the Sahel, which leads to increased soil moisture and, in turn, leads to a better agreement of the simulated surface latent heat release in summer with observations, reaching 100 W/m^2 from July to September and leading to more water recycling. As a result the sensible heat flux decreases by 40 W/m^2 during the monsoon season, in better agreement with the observations. However, nudging has little impact on the sensible flux during the dry season when the sensible flux remains overestimated. In the absence of latent heat flux and on a multiday basis (so that G cancels), the sensible heat flux is in balance with the net radiation. So, the overestimation of H should be associated with an overestimation of R_{net} . This is confirmed by Figure 5, in which the net radiation and its decomposition into short and long-wave components ($R_{net} = SW_{net} + LW_{net}$) observed at the different sites are compared with the free and nudged simulations.

Figure 5 further shows that nudging leads to a better representation of the seasonal behavior of the net infrared fluxes (LW_{net}) compared to local observations. The correction due to nudging is the strongest

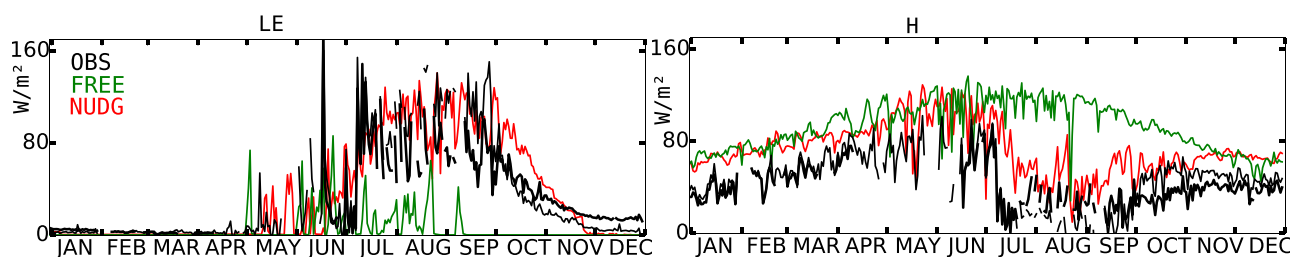


Figure 4. Time series of the (left) daily latent heat flux and (right) sensible heat flux for 2006 at Wankama. Local observations (black) are compared with the NUDG (red) and FREE (green) simulations using the STD physics.

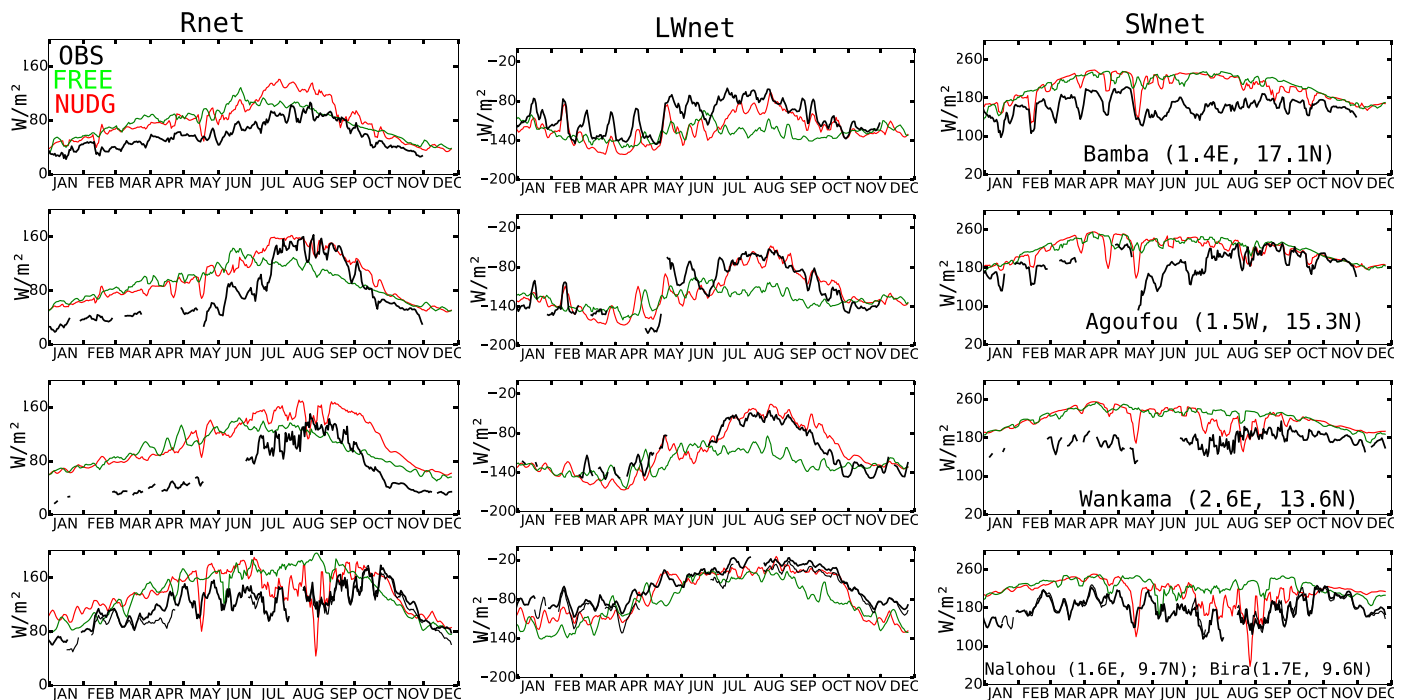


Figure 5. Time series of the 3 day running mean net radiation (left column), long wave net radiation (middle column) and solar net radiation (right column) for year 2006 at the Bamba, Agoufou, Wankama, Nalohou and Bira (in W/m^2) stations from top to bottom panels respectively. Local observations (black) are compared with the NUDG (red) and FREE (green) simulations with the STD physics. All the radiative fluxes are counted positive downward.

during the rainy season where the net infrared flux is increased (decreased in absolute value) by about 30 to 60 W/m^2 depending on the station considered.

Two explanations can be mentioned for the increase of the net LW radiation with nudging during the rain season (concentrating on Agoufou in July–August, where the impact is strongest). On the one hand, from an atmospheric radiation perspective, the increased atmospheric moisture increases the greenhouse effect. The mean free path of photons is shorter. If the vertical temperature structure does not change, the net radiation becomes less negative. On the other hand, starting from the surface energy balance, nudging helps to bring rainfall to the station, in turn increasing soil moisture and surface evaporation. This results in a cooling of the surface by typically 5–10 K. So the upward LW radiation decreases (as seen in Figure 6a) by about 60 W/m^2 , consistently with $\delta \ln(\sigma T^4) = 4\delta \ln(T)$. However, the atmospheric temperature decreases as well, by 10 K in the first 3 km or so (Figure 6c) due to the strong surface-atmosphere coupling. This colder air should emit less infrared radiation down to the surface. It is not the case in fact because the radiation is coming from lower in the atmosphere, as explained above. So that, at the end, the incoming LW radiation is not affected by nudging during the rain season (Figure 6b).

In fact, whatever the origin of a change in temperature, either at the surface or within the atmosphere, the surface-atmosphere coupling will rapidly reduce the temperature contrast, and reduce in turn the change in net LW radiation. At the end, the opacity variations (which are very large here because of the very large variations in air moisture) explain most of the fluctuations of the net LW radiation (Betts, 2004). Figure 6d shows indeed the strong correlation between q_{2m} (here a proxy of atmospheric humidity) and net LW radiation for the Agoufou site.

Note that clouds may contribute as well to the increased opacity. However, for the model at least, the cloud radiative forcing during the rain season is of 15 W/m^2 only. So it explains only one fourth of the total LW increase.

Due to the good representation of q_{2m} , the NUDG simulation correctly captures the isolated peaks in net LW radiation in winter and late Spring over Sahel (Figure 5), associated with synoptic scale moisture intrusions, as well as the increase of the net LW radiation (decrease of its absolute value) with the arrival of the monsoon flow in May.

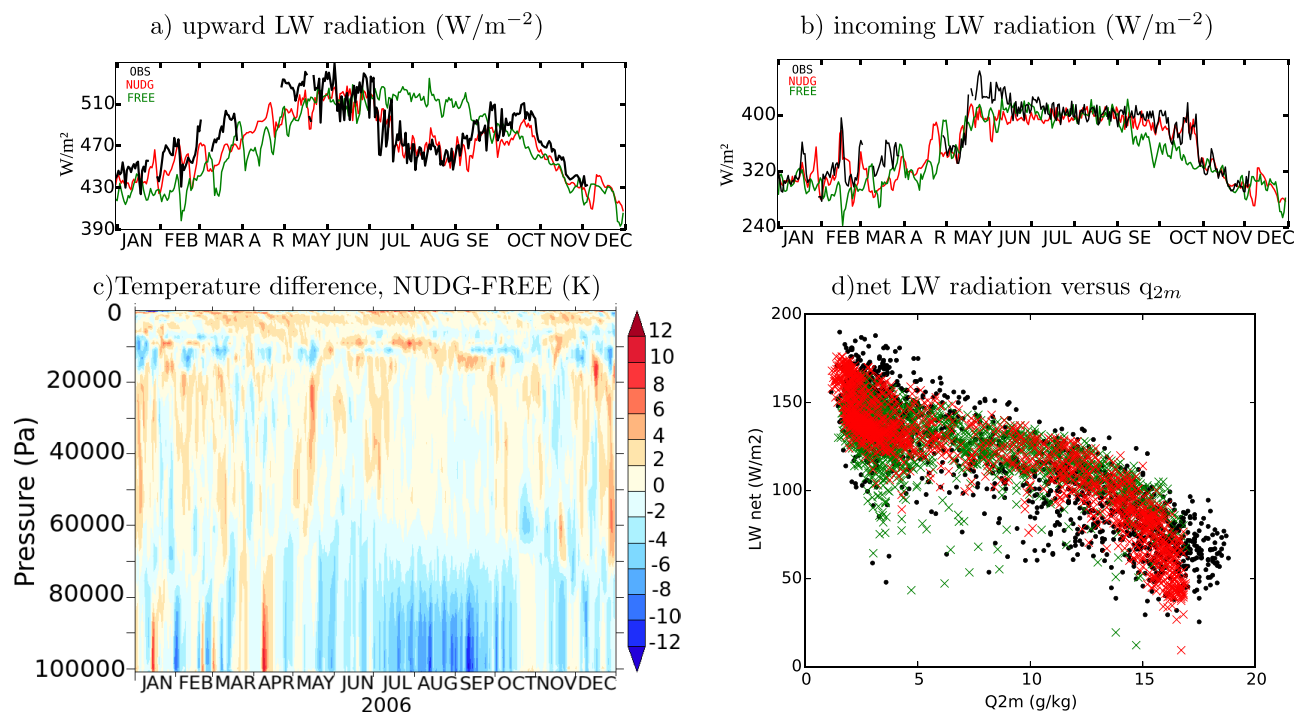


Figure 6. Water vapor and LW radiation in the NUDG and FREE configuration with the STD physics at Agoufou. (a) Upward and (b) downward LW radiation at surface (in W/m^{-2}), comparing observation (black) with FREE (green) and NUDG (red) simulation. (c) Time evolution of the difference of the vertical temperature profiles (NUDG minus FREE) and (d), scatter plot of q_{2m} and net LW for the observations (black), and FREE (green) and NUDG (red) simulations. The scatter plot was obtained by cumulating all the data for all the years available for observations, and the 4 nearest grid point for the model, leading to about 1500 values in both cases.

The net short wave radiation (SW_{net}) is overestimated compared to observations at all stations. The above-mentioned peaks are also visible (reduction of SW_{net}) in the observations. Nudging helps producing similar synoptic peaks in the simulations but this improvement in the simulations is not as clear for SW_{net} as it is for q_{2m} . During the rainy season nudging contributes to a reduction of the overestimation of SW_{net} at all sites, although the magnitude of this reduction weakens from south to north. On average, nudging leads to a reduced bias at Bamba by less than $10 W/m^2$ and by about $20 W/m^2$ at Nahoulou.

As a result, the nudging technique leads to an improvement of the representation of the seasonal cycle of the radiative budget at the surface but large biases persist. Before the monsoon onset, R_{net} is overestimated at all sites and this bias associated with a bias in SW_{net} is maximum at Wankama. During the rainy season, the nudging technique leads to an improvement of the phasing of the maximum of R_{net} in August over Sahel, as well as an improvement of the representation of the retreat phase from October to December, except at Wankama where R_{net} is overestimated by about $40 W/m^2$. Altogether, the remaining biases of R_{net} in the nudged simulations are mainly explained by the SW_{net} biases.

4.2. Decomposition of the SW Biases

In order to better understand the origin of the SW_{net} biases, the daily evolution of the solar flux arriving at the surface (SW_{in}) and the daily evolution of the surface albedo are considered separately (see Figure 7). The simulation with STD physics and nudging shows sudden drops of SW_{in} consistent with observations. Drops of SW_{in} are less numerous and not as sudden in the FREE simulations. Bouniol et al. (2012) derive the seasonal cycle of cloud occurrences and types as well as their radiative impact over West-Africa combining observations from the ARM mobile facility in Niamey and CALIPSO data collected in 2006. They emphasize the importance of mid-level clouds that have a strong impact in both the SW and LW radiation and that are present all year long, in particular during the spring when the other types of clouds are less numerous. Additionally, Roehrig et al. (2013) show that low and mid-level clouds are better represented in the STD than in the OLD version of LMDZ (IPSL-CM5B-LR compared to IPSL-CM5A-LR in their Figure 7). We do see

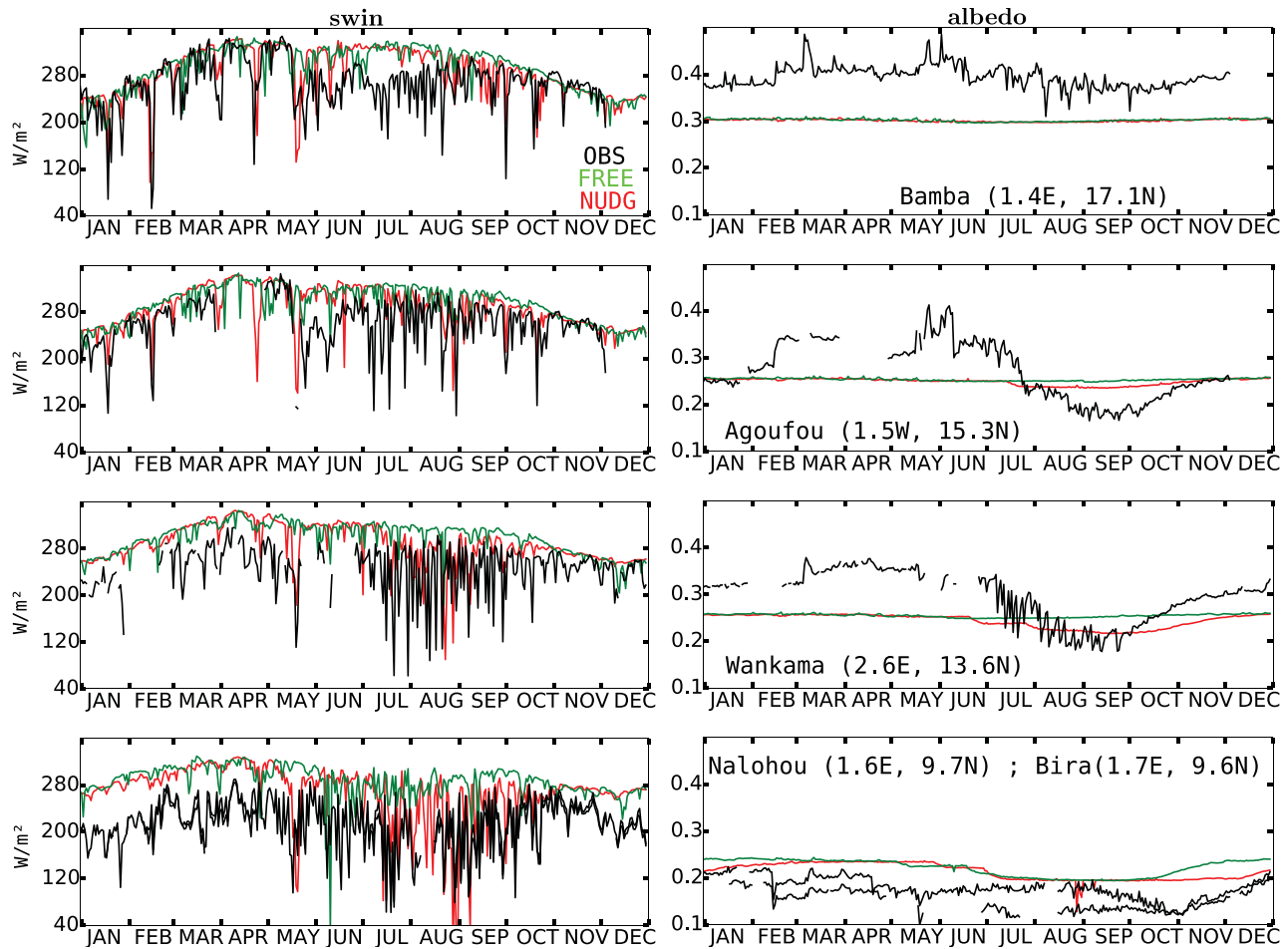


Figure 7. Time series of the daily surface incoming solar radiation (W/m^2 , left column) and the surface albedo (right column) for year 2006 at the Bamba, Agoufou, Wankama, Nalohou and Bira stations, from top to bottom plot respectively. Local observations (black) are compared with the NUDG (red) and FREE (green) simulations with the STD physics.

that the peaks in SW_{in} are better represented with the STD version of the model. In the model, those peaks are clearly attributable to the presence of mid-level clouds (Figure 8). However, despite this improvement, the solar flux reaching the surface is still overestimated. The overestimation is particularly strong during the rainy season. This overestimation is less in the OLD version of the model, which simulates more high-level clouds, suggesting an underestimation of high-level clouds in the STD version of the model. So even if the rainfall is stronger in the NUDG configuration thanks to the better ITCZ position, the clouds (and in particular high clouds) associated with this rainfall are probably strongly underestimated.

During the dry season, the simulated daily fluxes are in close agreement with observations at Bamba (Figure 8). Further south at Agoufou SW_{in} is overestimated by about $30 W/m^2$ before mid-May and this bias amplifies southward. This may be caused by an underestimation of aerosols and/or clouds in the model.

The surface albedo in the observations varies slightly in Bamba while it decreases at Agoufou and Wankama during the rainy season due to the subsequent growth of the vegetation (mainly grass), which is darker than the underlying bright soil. The bare soil fraction at Bamba during the rainy season being close to 1 (a Leaf Area Index or LAI of 0.01 was measured in 21 October 2006, Timouk et al., 2009), the albedo value stays very close to that of bare soil. At Agoufou and Wankama, the bare soil fraction during the rainy season being respectively of about 45% (Mougin et al., 2014) and 70% (for an average LAI of 0.85, Boulain et al., 2009), the albedo values drop during this period (Ramier et al., 2009; Samain et al., 2008). In the model, the surface albedo in the Sahelian zone is underestimated: throughout the year at Bamba (its value is about 0.38 in the observations and 0.28 in the model) and before the monsoon onset at Agoufou and Wankama.

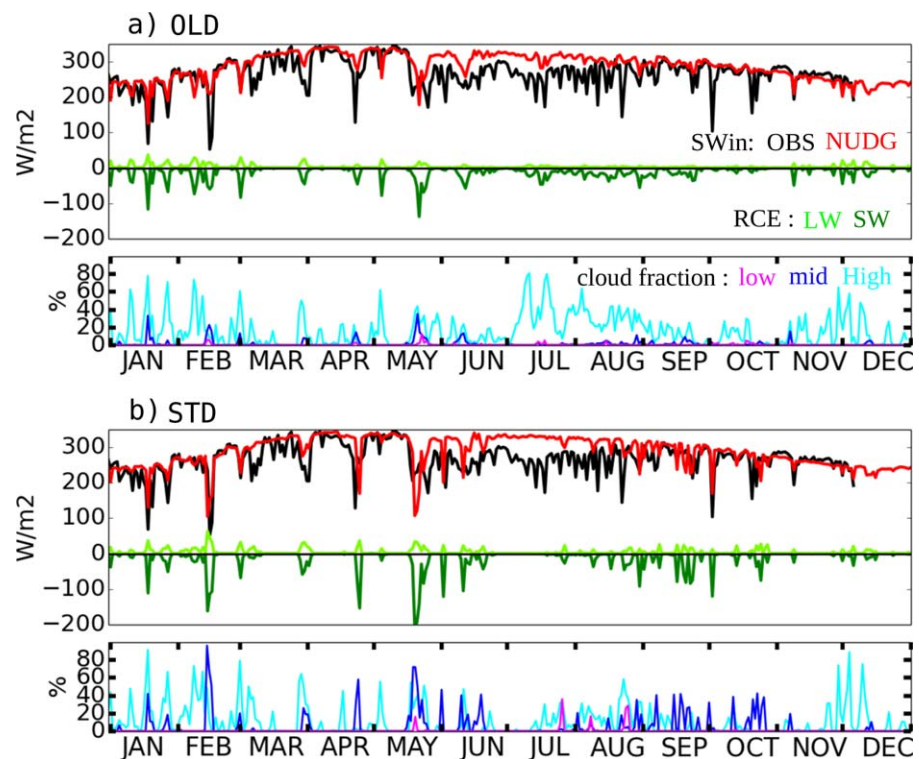


Figure 8. Time series of the observed daily solar flux (in W/m^2) reaching the surface at Bamba (black line) compared with the NUDG simulations (red) for the STD (top) and the OLD physics (bottom). Time series of the daily long-wave (light green) and short-wave (dark green) radiative effect (in W/m^2) of simulated clouds. Time series of the simulated daily low- (magenta), middle- (blue) and high- (cyan) level cloudiness (in %).

This indicates that the albedo of bare soil is generally underestimated over the Sahel in the model. At Agoufou and Wankama, the model poorly reproduces the albedo seasonal cycle despite nudging and the surface albedo in the middle of the rainy season is overestimated. This indicates either an underestimation of the fraction occupied by the vegetation or an overestimation of the albedo of the vegetation itself. In the Sudanian region, the surface albedo is slightly overestimated by 3.5% in the NUDG simulation.

The wrong representation of albedo can cause, weaken, or amplify the SW_{in} bias (i.e., SW_{net} overestimation during the dry season). The contribution of SW_{in} to the SW_{net} bias is found to be larger when moving southward. During the rainy season, the overestimation of the surface albedo at the three southernmost stations partly compensates for the overestimated SW_{in} (probably related to a lack of clouds associated with convection).

The albedo biases identified here motivated a revisit of the surface albedo for the version of the IPSL coupled model under development for CMIP6, both the background albedo of bare soils and albedo of the various vegetation types.

From this analysis the biases in net radiation at the surface in the model can be attributed to errors in moisture advection by the large-scale dynamics on the one hand (corrected by nudging) and to a misrepresentation of surface albedo, aerosols and clouds on the other hand (that relies on model physics).

4.3. Temperature Biases

Observed and simulated 2 m temperature (T_{2m}) are compared in Figure 9. The 2 m temperature is strongly coupled to the surface temperature during daytime, and is sensitive to the radiative and turbulent exchanges between the surface and the atmosphere (Ait-Mesbah et al., 2015).

Beyond the phasing of the simulated and observed synoptic variability, the main effect of nudging is a reduction of T_{2m} during the rainy season, especially at Agoufou and Nalohou, leading to a much better representation of the seasonal behavior of T_{2m} . This correction is due to the increased evaporative cooling

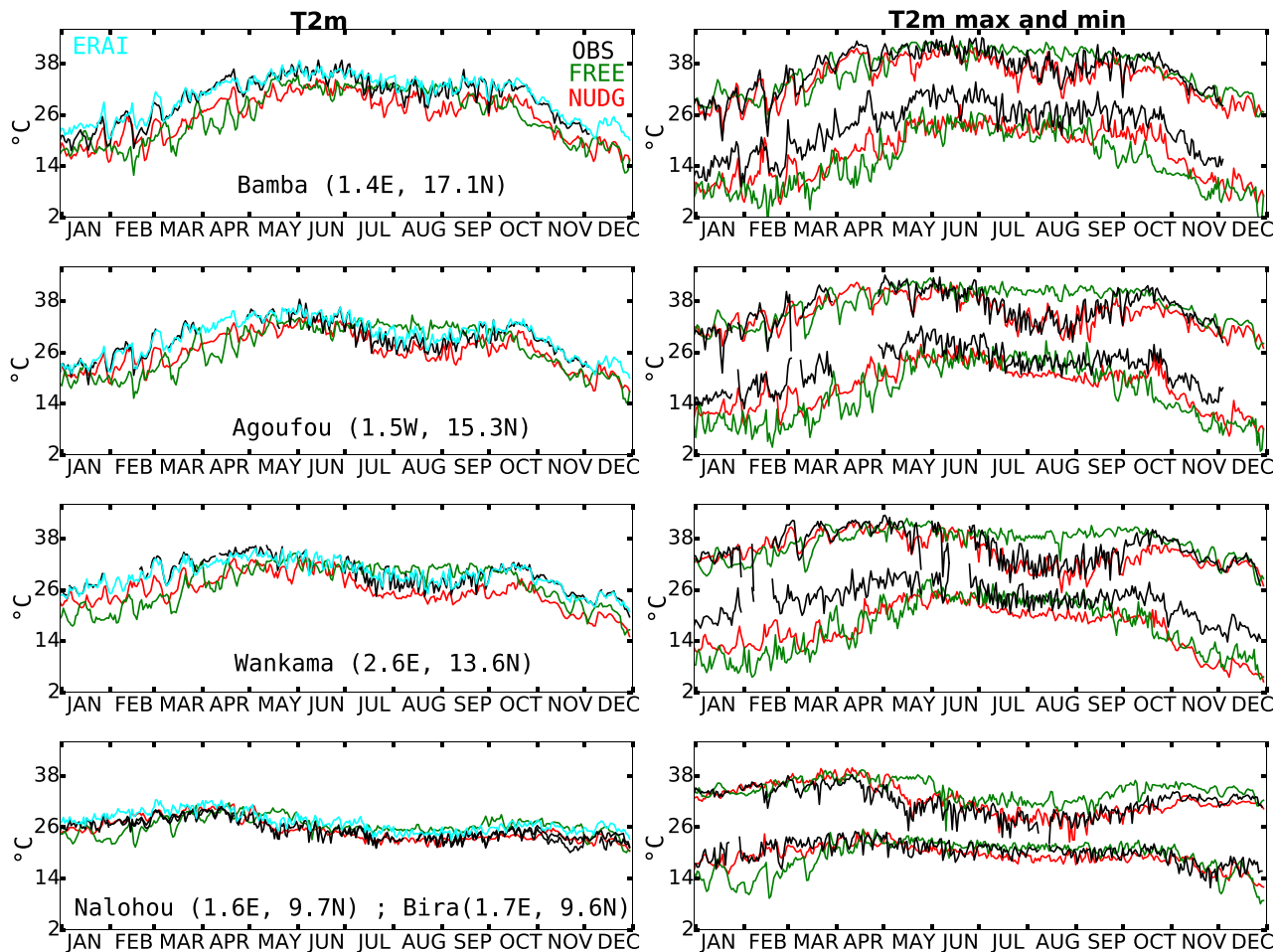


Figure 9. Time series of the daily 2 m temperature (in C, left column) and of the daily maximum and minimum 2 m temperature (right column) for year 2006 at the Bamba, Agoufou, Wankama, and Nalohou stations from top to bottom respectively. Local observations (black) are compared with the NUDG (red) and FREE (green) simulations with the STD physics.

discussed above. The effect on T_{2m} mainly comes from a reduction of the daytime temperature as seen from the comparisons of the daily minimum and maximum values of T_{2m} , T_{2m}^{\min} and T_{2m}^{\max} (Figure 9, right column). With nudging, T_{2m} is reasonably well simulated at the four available stations.

Considering the nudged simulations only, a systematic cold bias at the three Sahelian stations remains despite the overestimated SW_{net} and R_{net} (see Figure 9). This cold bias is a night-time bias as seen from the strong underestimation of T_{2m}^{\min} at the same stations (Figure 9, right column).

We can suspect different origins for this excessive temperature drop during night-time, e.g., an underestimation of the greenhouse effect, an overestimation of heat conduction below the surface or an underestimation of turbulent mixing in the lowest atmospheric layers. Note that the bias is slightly reduced with the OLD physics as seen in Figure 10 for the Bamba station. The explanation is rather direct since the model for turbulent diffusion used in the OLD physics was much more “viscous” than the Mellor and Yamada approach used in the STD version. We have other indications however that the STD version much better represents stable boundary layers. So probably the better results of the OLD simulation comes from a compensation of error with other aspects of the model physics.

In fact, the good agreement with observation for the maximum temperature may be even more puzzling, in view of the excessive SW_{net} radiation absorbed at the surface. This may suggest here also that compensating errors are at work. Longwave radiation, turbulence, but also boundary layer convection, may be involved during daytime.

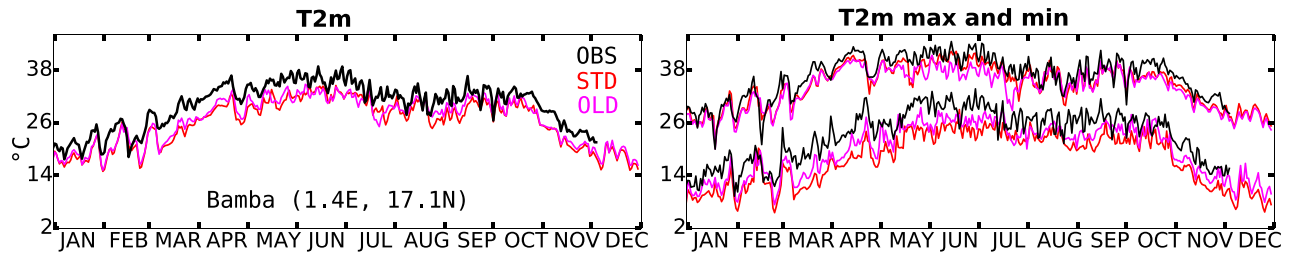


Figure 10. Time series of the daily 2 m temperature (in C, left column) and of the daily maximum and minimum 2 m temperature (right column) for year 2006 at the Bamba station. Local observations (black) are compared with the nudged simulations for the STD (red, same curve as in the top row of Figure 9) and OLD (magenta) physics.

In the next section, the aforementioned possible origins of temperature and net radiation biases are further investigated by analyzing a series of sensitivity experiments.

5. Pathways Toward Bias Reduction

In this section, we aim to more precisely identify the origins of the temperature and radiation biases highlighted in section 4 in order to improve the STD version of the model in the NUDG configuration. Those experiments were designed as pathways for model improvement and tuning in the frame of the development of the CMIP6 version of the IPSL climate model. We first address the origins of the temperature biases before investigating those of the albedo and net radiation biases.

5.1. Sensitivity of Night Time Temperature to Thermal Inertia

The sensitivity of the temperature to soil thermal properties is analyzed first.

For a vertically homogeneous soil, the thermal behavior of the soil is controlled by a unique parameter, the thermal inertia $I = \sqrt{KC}$, where K and C are the thermal conductivity and the heat capacity respectively. In the standard version of the ORCHIDEE surface model, these parameters depend on the soil moisture as follows:

$$K = K_{dry} + Sr(K_{wet} - K_{dry})$$

$$C = C_{dry} + Sr(C_{wet} - C_{dry})$$

where the degree of soil saturation Sr is the ratio of the soil moisture to its maximum value for a saturated soil, $K_{dry} = 0.4 \text{ W} \cdot \text{m}^{-1} \cdot \text{K}^{-1}$ and $C_{dry} = 1.8 \times 10^6 \text{ J} \cdot \text{kg}^{-1} \cdot \text{K}^{-1}$ (resp. $K_{wet} = 1.8 \text{ W} \cdot \text{m}^{-1} \cdot \text{K}^{-1}$ and $C_{wet} = 3.03 \times 10^6 \text{ J} \cdot \text{kg}^{-1} \cdot \text{K}^{-1}$) are the thermal conductivity and heat capacity of a completely dry (resp. saturated) soil, taken constant over the Sahel in the current version of the ORCHIDEE model.

We choose to explore the sensitivity to thermal inertia by imposing a constant value of Sr all year long. This allows both to test extreme values of the soil thermal inertia by imposing either a fully saturated ($Sr = 1$) or dry soil ($Sr = 0$), and to test the behavior of the seasonal dependency to soil humidity by comparing simulations with constant or varying Sr . The $Sr = 1$ case corresponds to a large thermal inertia $I = 2335$ (USI) and the $Sr = 0$ case to $I = 849$ (USI). An intermediate simulation was also performed with $Sr = 0.5$.

The model value of the thermal conductivity for dry soil over the Sahel is consistent with the terrain measurements which suggest values between 0.25 and 0.4 W/m/K for dry soils and 1.4 to 2 for saturated soils. The heat capacity value is probably somewhat overestimated, the literature suggesting values of 1.2×10^6 for dry soil, to 1.84×10^6 J/kg/K for wet soils, leading to thermal inertia values of typically 500–800 USI for dry soil and 2000–3000 USI for fully saturated soils (Murray & Verhoef, 2007; Verhoef et al., 2012). The expected value of Sr over the Sahel is going from 0 in the dry season to 0.4 after rainfall events. For $Sr = 0.4$, the value computed by the model, $I = 1490$ USI, is close to the values reported in the literature.

Consistently with the results of Ait-Mesbah et al. (2015) and Sandu et al. (2013), the night-time temperature increases significantly with increasing values of the soil thermal inertia (Figure 11). In comparison, the

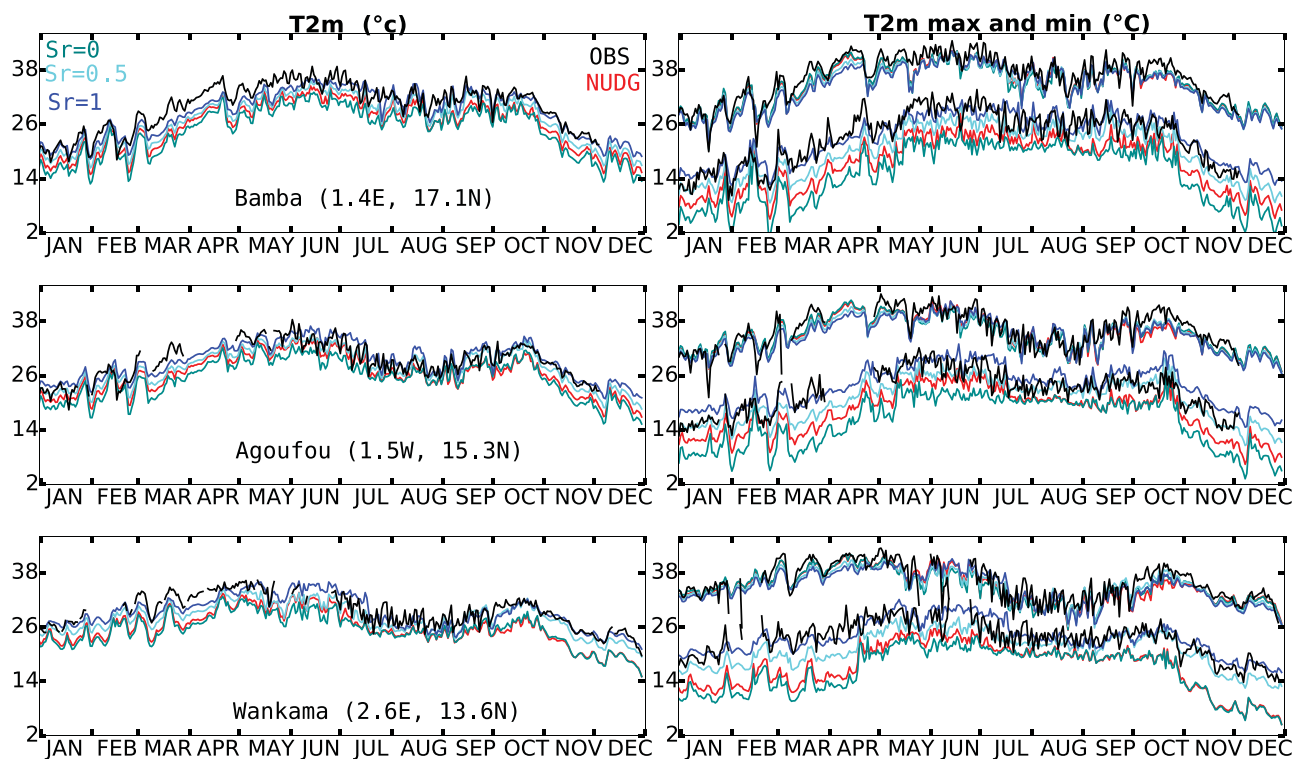


Figure 11. Time series of the daily 2 m temperature (in C, left column) and of the daily maximum and minimum 2 m temperature (right column) for different values of the surface thermal inertia corresponding to dimensionless saturation ratio: $Sr = 0$ (dark cyan), $Sr = 0.5$ (cyan) and $Sr = 1$ (blue) in the control simulation (red), in the in-situ observations (black) for Bamba (top row), Agoufou (middle row) and Wankama (bottom row) sites for year 2006.

maximum daytime temperature varies only slightly. Globally speaking, the best simulation of T_{2m}^{min} is obtained for a saturated soil $Sr = 1$.

For the dry season at least, such a large thermal inertia is not compatible with the values reported in the literature, while for the rainy season, T_{2m}^{min} is quite well represented for $Sr = 0.5$, i.e., for a large but acceptable value of the soil thermal inertia. Unexpectedly the control NUDG simulation, in which Sr is computed interactively, is closer to the $Sr = 0$ simulation during the rainy season and closer to the $Sr = 0.5$ simulation during the dry season. This result in fact points to an erroneous behavior of the model itself, which happens to have different origins during the dry or the wet season. The version of the ORCHIDEE model used here is a 1.5-layer model. It is made of one main layer which reacts as a water bucket. It is filled by rainfall and evaporates with a resistance that depends on the height of water in the bucket and on the characteristics of the vegetation. In addition to this main layer, an additional layer is created intermittently after rainfall events to handle fast processes. In this case, the surface layer is driven by rainfall and evaporation and exchanges with the main layer below. Sr is computed simply as the ratio of the bucket water content to its maximum value. During the dry season, the model acts as a bucket. The water from that bucket is far from the surface and the evaporation cancels due to the functions that control the resistance to evaporation and Sr should probably go to zero. However, it does not decrease below 0.3. At the opposite, during the rainy season, it turns out that Sr is underestimated because of a bug, Sr being computed using the ratio of the humidity in the first layer to the maximum content of the full soil model.

Altogether, an underestimated thermal inertia due to the aforementioned problem could explain in part the underestimation of the night-time temperature during the rain season. During the dry season, the thermal inertia is probably strongly overestimated by the model, both because of the wrong model behavior and because of soil constants for dry soil which are a bit overestimated. So the temperature cold bias should probably be even larger with a better soil model, probably pointing to a problem in the representation of the other processes that control the decrease of surface temperature during the night: turbulence and long-wave radiation (Aït-Mesbah et al., 2015).

The sensitivity shown here points to the importance of the representation of the soil thermal properties and of their dependence to soil moisture. For the CMIP6 version, the IPSL model will use a 11-layer discretized model for water transfer in the soil, coupled to a thermal conduction model that uses the same vertical discretization (Wang et al., 2016).

5.2. Sensitivity of Night-Time Temperature to Turbulent Mixing

The sensitivity of temperature to the near surface turbulent mixing is explored by varying either the surface roughness (Z_0) or the mixing length $l = \max(l_{\min}, l_*)$ where l_{\min} is a threshold and l_* is a mixing length calculated with the Blackadar (1962) formula.

In the CMIP5 version of LMDZ, there is no distinction between the roughness lengths for momentum (Z_{0m}) and for thermodynamic variables (Z_{0h}), i.e., $Z_{0,h} = Z_{0,m}$ although it is generally accepted that $Z_{0,h} \ll Z_{0,m}$. A sensitivity experiment is run by imposing $Z_{0,h} = Z_{0,m}/10$ (a generally accepted value for this ratio; e.g., Garrat (1992)). The effect of this change happens to be weak and is not documented here.

The impact of changing the threshold value for the minimum mixing length (l_{\min}) from 1 to 20 m is shown in Figure 12. The impact of increasing l_{\min} is qualitatively similar, although weaker, to that of increasing the thermal inertia. It reduces the night-time biases by about 2°C and the T_{2m} mean bias by 0.8°C . This test confirms that the too cold night-time temperature may be in part due to an underestimated turbulence in stable nocturnal conditions. A correct representation of the stable boundary layer remains a challenge for boundary layer parameterizations (Bosveld et al., 2014; Lohou et al., 2014).

5.3. Origin of Albedo Biases

In this section, sensitivity experiments are performed to understand the origin of the misrepresentation of surface albedo (α) that remains even in the NUDG simulations with STD physics, and to document the

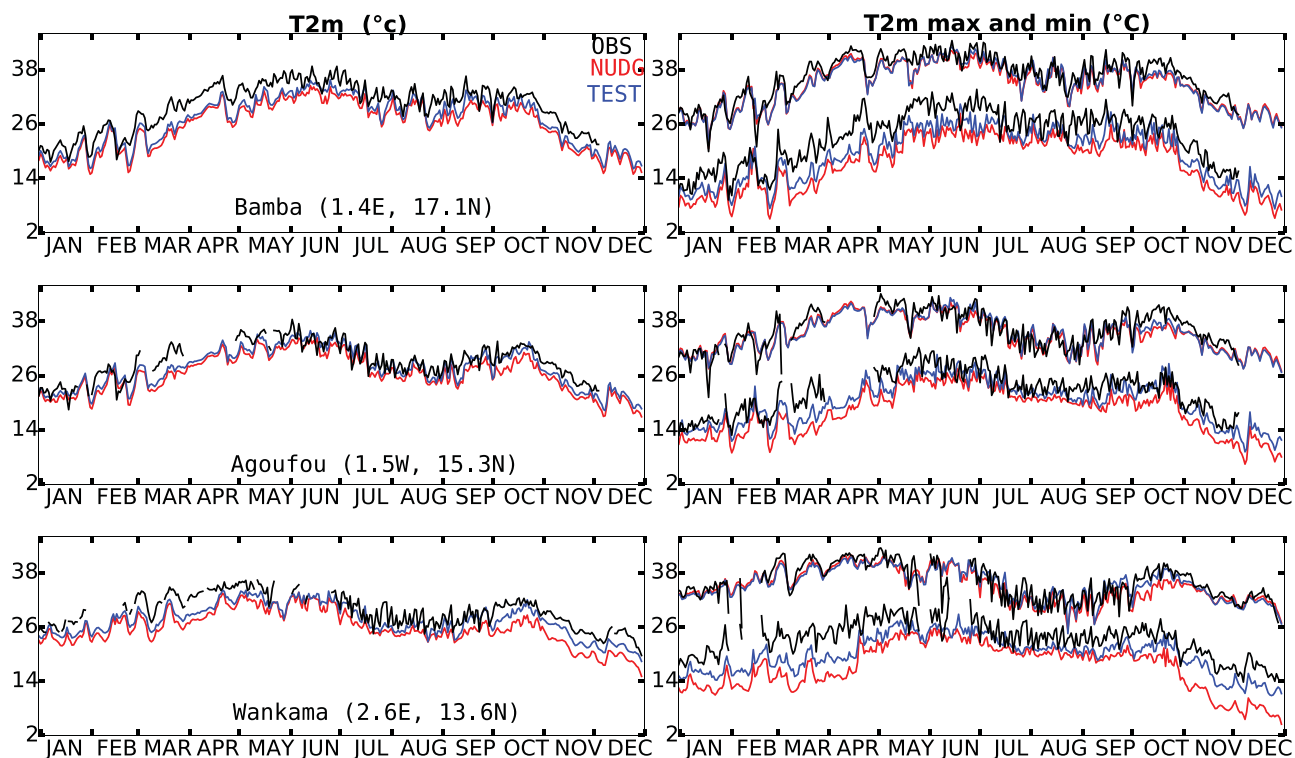


Figure 12. Time series of the daily 2 m temperature (T_{2m} , in C, left column) and of its minimum and maximum daily values (right column) in a sensitivity experiment with increased minimum turbulent mixing length (blue) compared to the control simulation (red) and to the in situ data (black) for Bamba (top row), Agoufou (middle row) and Wankama (bottom row) sites for year 2006.

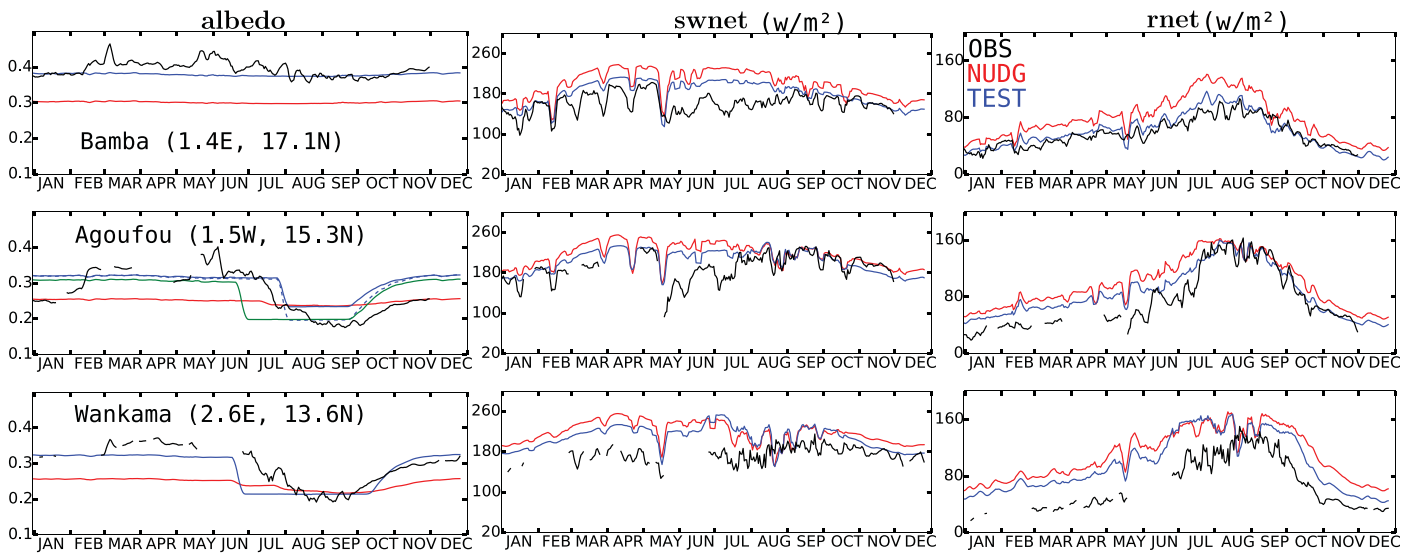


Figure 13. Time series (3 day running mean) of the diurnal averaged albedo (left column), solar net radiation (middle column) and net radiation (right column) for Bamba (top row), Agoufou (middle row) and Wankama (bottom row) sites for year 2006 for the local observations (black) and in the control simulation (red) and sensitivity experiment with modified albedo (blue). In the second panel on the left column, the albedo estimation from the sensitivity experiment in which the weight attributed to the albedo of bare soil in summer is changed from 50% to 30% (dash blue curve) as well as the albedo obtained from western nearest neighbor grid-cell (green curve, 3.8 ° W, 15.3° N) are also shown.

impact of albedo errors on the surface energy budget. During the dry season, the albedo value is high and close to bare soil albedo of deserts (Tsvetsinskaya et al., 2002). During the rainy season, it decreases as vegetation grows, as explained earlier. In the model, the albedo is expressed as:

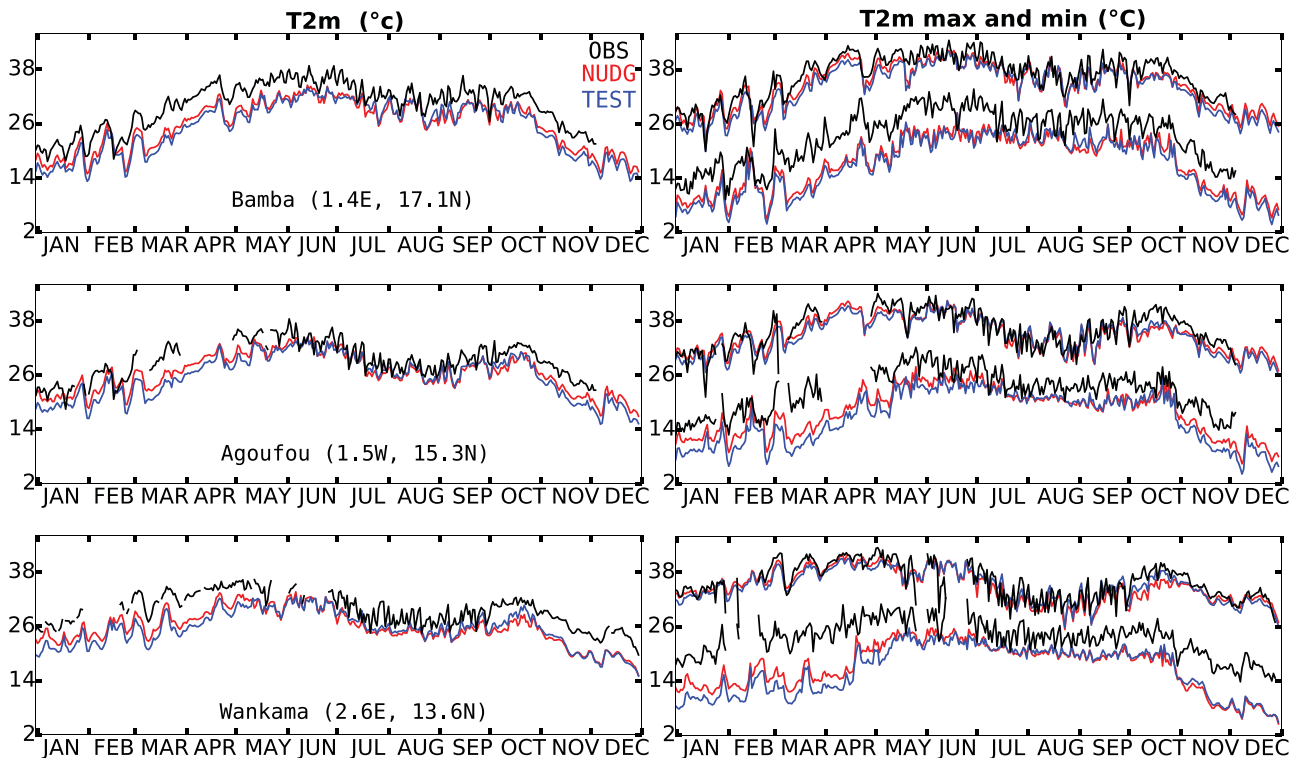


Figure 14. Time series of the daily 2 m temperature (T_{2m} , in C, left column) and of its minimum and maximum daily values (right column) for Bamba (top row), Agoufou (middle row) and Wankama (bottom row) sites for year 2006 in the in situ observations (black) and in the control simulation (red) and sensitivity experiment with modified albedo (blue).

$$\alpha = \alpha_{bare} \left[f_{bare} + \sum (f_{pi}(1 - \beta(Pi, t))) \right] + \sum (\alpha_{pi} f_{pi} \beta(Pi, t)) \quad (2)$$

with $\beta(Pi, t) = 1 - \exp[-k LAI(Pi, t)]$, $0 < \beta(Pi, t) < 1$, $0 < k < 1$. f_{bare} is the fraction of the grid cell that is always bare soil, Pi is the plant functional type, f_{pi} is the maximum fraction covered by Pi in the grid point and $f_{pi} \beta(Pi, t)$ represents the fraction of the surface effectively covered by leaves, k is the extinction coefficient within the canopy fixed at 0.5 in the model standard version. In the model used here the 13 plants functional types are defined, three of which are effectively present over Sahel (two types of grass and one type of crop). In the version used here, the fraction of each plant functional type is imposed once for all in each grid-cell (no dynamic vegetation) but the leaf (or grass) growth is computed interactively with the meteorology by activating the STOMATE component of the ORCHIDEE model.

A sensitivity experiment is performed where the albedo is changed in a Sahelian zone defined as a rectangular box (17° W-10° E; 12° N-20° N). The bare soil albedo is increased by a constant factor of 1.26 to better match the observations during the dry season. The albedo of the Savannah plant functional type is decreased from 0.2 to 0.15 in order to decrease the simulated albedo during the rainy season. A value of 0.15 is in fact more consistent with in situ measurements at maximum canopy cover (Ramier et al., 2009;

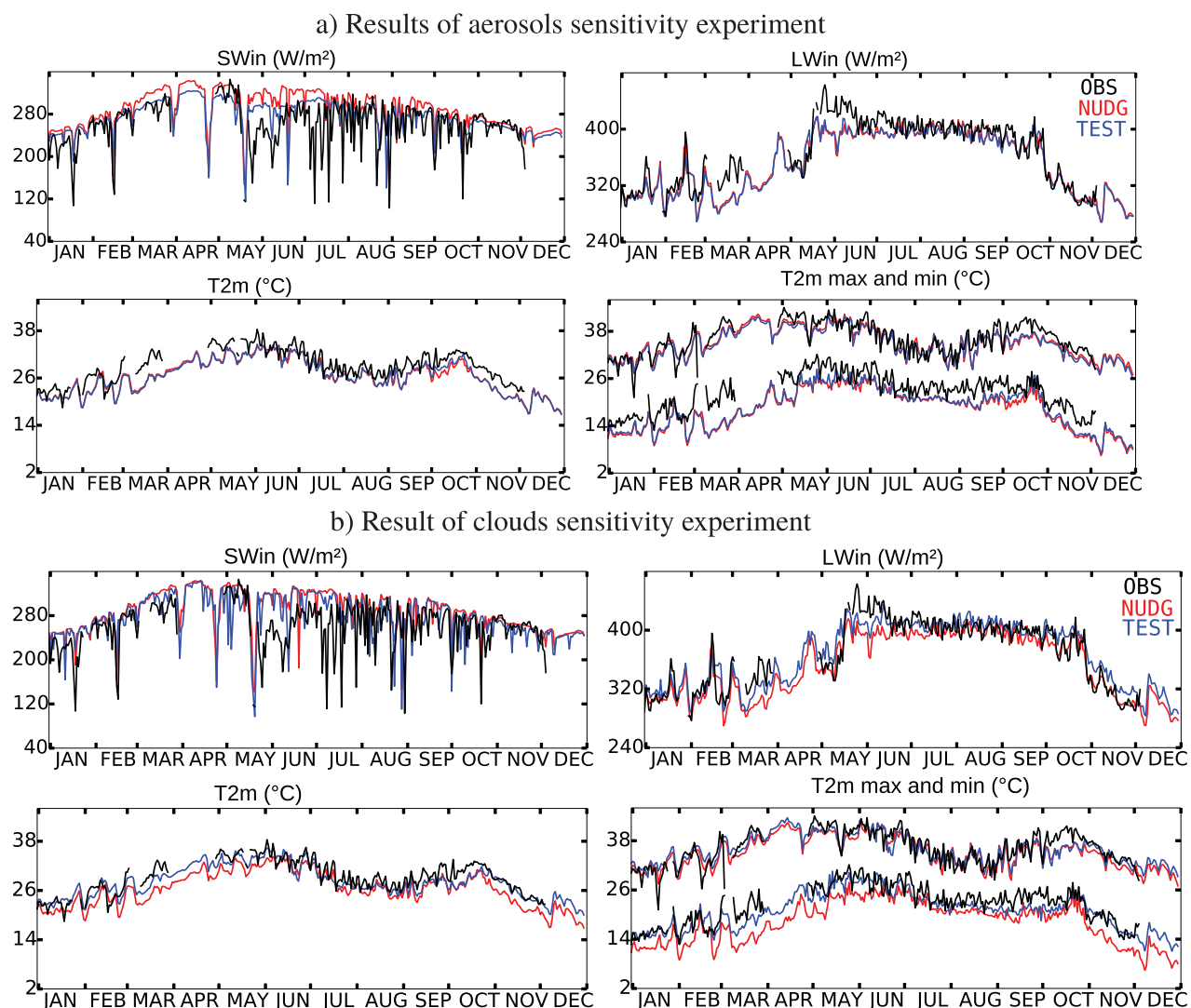


Figure 15. Surface incoming solar and long-wave radiations (in W/m^2), 2 m temperature (in C, mean, min and max) at the Agoufou station for 2006 in the sensitivity experiments (blue) to the (a) aerosols and (b) clouds, in the daily local observations (black) and in the control simulation (red).

Samain et al., 2008) and is close to the lower values reported for grassland and the medium value for savannas (Cescatti et al., 2012). The classical formulation of β (LAI) is also changed to $(1 - \min(1, LAI(P_i, t)))$. This extreme approximation consists in assuming that all leaves lie side by side on the surface until they reach f_{pi} . Note that the darkening of the Sahel during the monsoon season may also be affected by the direct effect of soil moisture on the bare soil albedo. This dependency of bare soil albedo to soil moisture, not activated in this version of the model, would probably not be strong enough to explain the discrepancy with the observed albedo. This process is in part responsible for the fast oscillations observed in the surface albedo at Wankama. The effect of moisture is weak and restricted to a short period of time after rainfall events (Ramier et al., 2009; Samain et al., 2008) (see Figure 8).

The effect of these albedo changes on the net and incoming solar radiation is shown in Figure 13 at Bamba, Agoufou and Wankama. At Bamba, the surface albedo variation between the dry and the rainy seasons is of the order of 1% in the observations so that correcting the surface albedo of bare soil alone is enough to match the observed surface albedo reasonably well. This leads to a bias reduction on SW^{net} in particular during the dry season where the simulated absorbed solar flux is very close to observations. This improvement leads to an improvement in the representation of the daily evolution of the net radiation budget (see Figure 13). However, this leads to a cooling of the surface and an increased cold bias (see Figure 14).

At Agoufou and Wankama, where the albedo variation is more pronounced between the dry and the rainy seasons (see Figure 13), the simulation with the modified albedo leads to a more realistic annual cycle of the albedo. However, despite those drastic changes in the surface albedo specification, the amplitude of the seasonal cycle of albedo at Agoufou is still underestimated. The agreement with observation could be improved when considering representativeness issues. The grid point containing the Agoufou station indeed contains

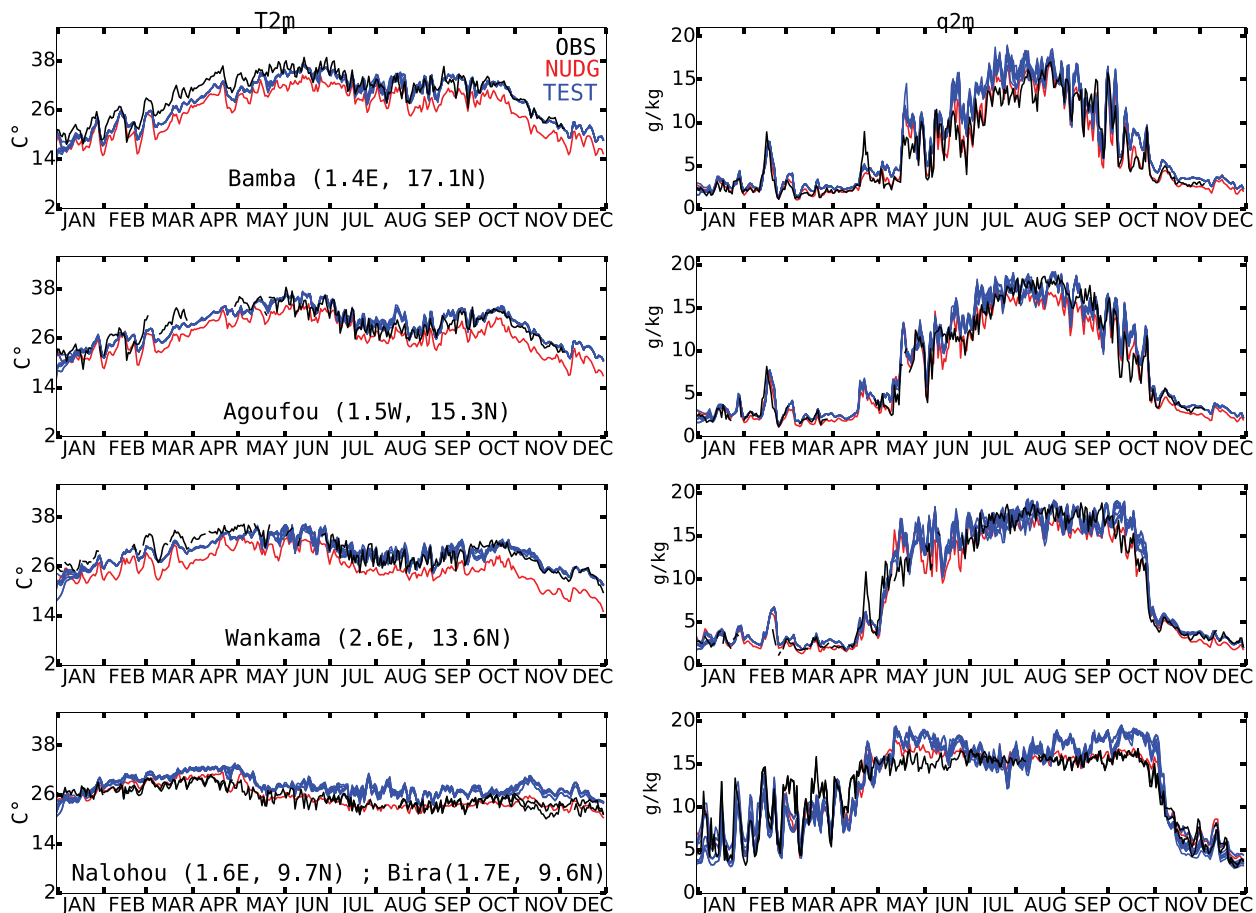


Figure 16. Sensitivity of the 2 m temperature (in C, left column) and the 2 m specific humidity (right column) to the combined surface thermal inertia, clouds and aerosols effect at Bamba, Agoufou, Wankama, Nalohou and Bira stations, from top to bottom panels respectively, for 2006 in the daily local observations (black), in the control simulation (red) and in the sensitivity experiments (blue).

50% of bare soil while the AMMA super-site where observations are sampled contains only 20% of bare soil. The surface albedo that would be simulated accounting for this different weighting is also shown on the figure (dash blue curve). The albedo value obtained in the sensitivity experiment is closer to observations in the rainy season even if it still drops at the beginning of August instead of mid-July. To explain this shift in season, observations are compared with the closest grid point west of the station, where rainfall starts earlier in July (this point is centered at 3.8° W). In this case the albedo decreases earlier. The difference of precipitation between the two grid points leads to a difference of LAI and induces in turn a shift on the seasonal cycle of albedo.

The improvement of the representation of the albedo cycle in Agoufou and Wankama reduces the SW_{net} bias there. Nevertheless, the net radiation budget is not significantly improved before the monsoon onset since the overestimation of SW_{net} is mainly due to the overestimation of SW_{in} at this period.

To summarize, these results clearly suggest that the standard version of the model suffers from an underestimated bare soil albedo and from an underestimated darkening effect by STOMATE during the rainy season, associated with the vegetation growth. Correcting the albedo helps improving the representation of radiative fluxes but tends to slightly increase the model cold bias (see Figure 14).

5.4. Sensitivity of the Surface Energy Budget to Atmospheric Opacity

The overestimation of the net radiation R_{net} over central and south Sahel before the monsoon onset is partly due to the overestimation of SW_{in} . The sensitivity of SW_{in} to clouds and aerosol is now considered. In the following experiments, only results at Agoufou are presented. The biases and effects of the sensitivity experiments are indeed similar at the other stations. The sensitivity of incoming radiation and 2 meter temperature to aerosol loading is first analyzed by increasing the atmospheric load by a factor of two for all

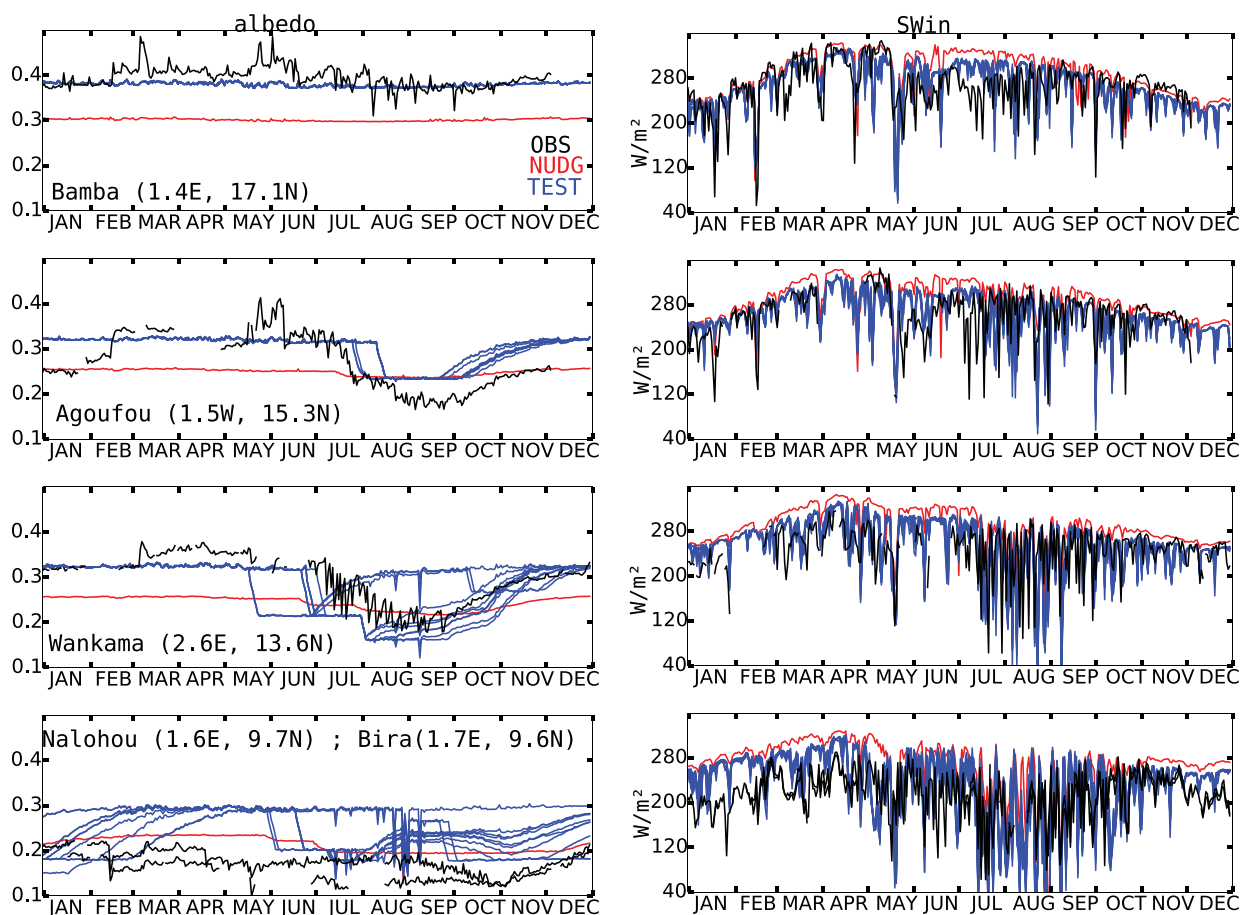


Figure 17. Sensitivity of surface albedo (left column) and surface short-wave incoming radiation (in W/m^2 , right column) to the combined surface thermal inertia, clouds and aerosols effect at Bamba, Agoufou, Wankama, NaLohou and Bira stations, from top to bottom panels respectively, for 2006 in the daily local observations (black), in the control simulation (red) and in the sensitivity experiments (blue).

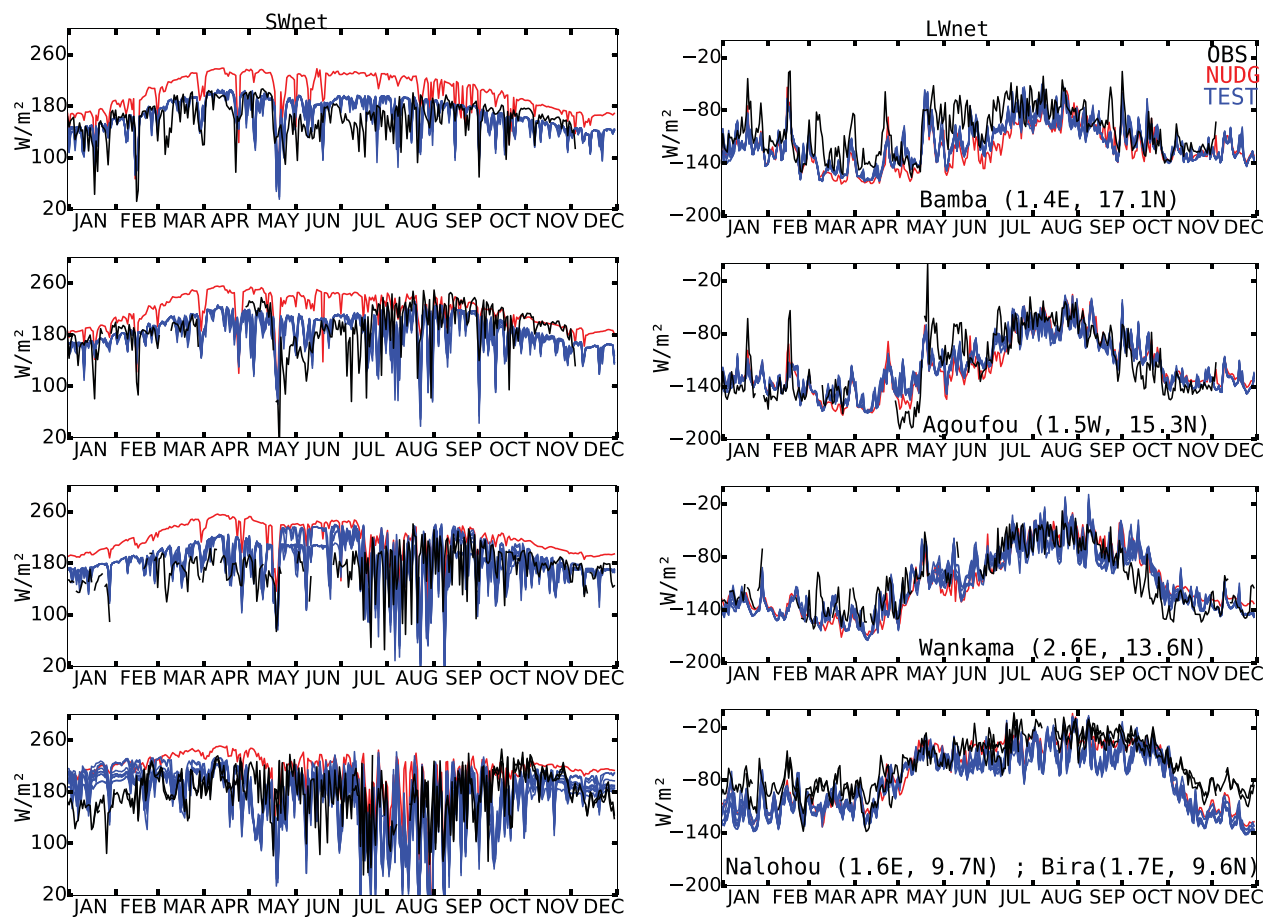


Figure 18. Sensitivity of the surface net solar radiation (left column) and the surface net long-wave radiation (right column) to the combined surface thermal inertia, clouds and aerosols effect at Bamba, Agoufou, Wankama, Nalohou and Bira stations, from top to bottom panels respectively, for 2006 in the daily local observations (black lines), in the control simulation (red lines) and in the sensitivity experiments (blue lines).

types of aerosols (Figure 15a). Increasing aerosol opacity is enough to significantly reduce the SW_{in} bias, except in June. Unlike albedo corrections, this reduction of incoming radiation decreases T_{2m} only weakly (e.g., by about 0.6° C in March, during the dry season).

The sensitivity of the same variables to cloud radiative effects (Figure 15b) is then analyzed by modifying the representation of clouds in the simulations. Results from section 4.2 suggest that the occurrence and radiative effect of high cirrus and anvil clouds are underestimated in our simulations. To increase the lifetime of high clouds and their radiative effect, we reduce the ice crystals fall speed by a factor of 2.7 in the STD simulation.

The parametrization of ice fall velocity is one of the most uncertain aspects of atmospheric models that affect most the clouds and the radiative balance. It is for instance the most crucial element controlling the life cycle of tropical anvil clouds in convection-permitting cloud simulations (Van Weverberg et al., 2013). It also strongly controls the total amount of high clouds in climate models, as well as their latitudinal distribution, and a scaling factor on the fall speed of ice crystals is often used during the final tuning process of climate models (Hourdin et al., 2017).

The fall velocity w_{iw} used in LMDZ is based on the formula proposed by Heymsfield and Donner (1990) in which $w_{iw} = \gamma_{iw} \times 3.29 \times (\rho q_{iw})^{0.16}$, q_{iw} being the ice water content and γ_{iw} a parameter introduced for the purpose of model tuning. The parameterization could probably be improved by incorporating a temperature dependence as suggested by Heymsfield et al. (2007) or by representing thin cirrus and thicker clouds generated by fresh convection differently as recommended by Schmitt and Heymsfield (2009).

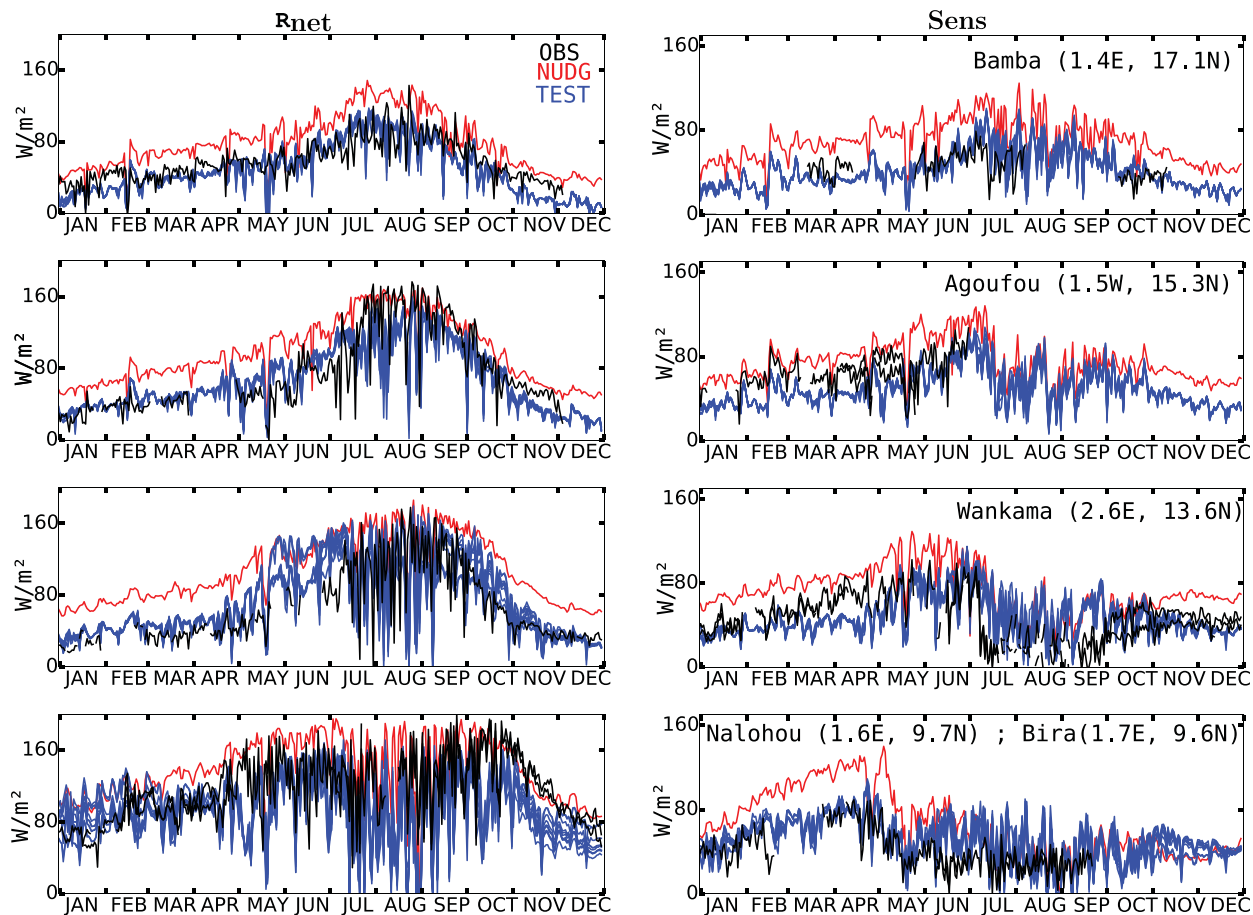


Figure 19. Sensitivity of the surface net radiation (left column) and the surface sensible heat flux (right column) to the combined surface thermal inertia, clouds and aerosols effect at Bamba, Agoufou, Wankama and Nalohou and Bira stations, from top to bottom panels respectively, for 2006 in the daily local observations (black lines), in the control simulation (red lines) and in the sensitivity experiments (blue lines).

Here, when reducing the value of the scaling factor γ_{ivr} the SW_{in} bias is slightly reduced and the model produces more variability of SW_{in} during the dry season in better agreement with the observations. By maintaining high clouds longer, the greenhouse effect is reinforced as can be seen in infrared radiation received at the surface (LW_{in}). The net effect is a significant reduction of the cold bias by 2° C.

In conclusion, the increase of the aerosol opacity reduces the SW_{in} biases without modifying surface air temperature significantly, while the increase of the life-time of high clouds improves both the SW_{in} daily variability and the 2m temperature in the model. Note that aerosols are prescribed as a mean seasonal cycle here but a model with interactive aerosols could increase the day-to-day variability of aerosols and radiation as well.

5.5. Combined Sensitivity Experiment

To estimate the improvement that could be expected from improved physics, a last sensitivity experiment is performed that combines all aforementioned tests on albedo formulation, aerosols, high clouds and thermal inertia for $Sr = 1$. The choice of $Sr = 1$ is extreme in terms of soil thermal properties and probably hides other model limitations.

The magnitude of these changes is further compared with the uncertainty range related to the internal variability of the nudged model by performing a set of 10 realizations of the sensitivity experiment differing by their initial conditions.

In the combined sensitivity experiment (blue line on Figure 16), the warming induced by modifying thermal inertia and ice crystals fall speed (see section 5.1 and 5.3) dominates the cooling induced by the modified

albedo (see section 5.2). Thus, although the changes lead to a warm bias in the Sudanese zone, the Sahelian cold bias of the NUDG simulation in the dry season is strongly reduced (by 1.6°C) before the monsoon onset and it is corrected after it. Analyzing the change in humidity in the independent sensitivity tests presented in the previous section (not shown), it appears that the reduction of the ice crystals fall speed is also responsible for the increase in q_{2m} seen in Figure 15 at Bamba and Nalohou stations. As shown in Figure 13, the albedo and its seasonal cycle in the Sahel are represented as in section 5.2, with the exception of Wankama. The SW_{in} biases are reduced or corrected and the SW_{in} variability is improved over all sites (Figure 17). As a result, the net solar radiation in the combined sensitivity experiment is much better represented during the year at all stations with the only exception of November–December at Agoufou (see Figure 18) where the SW_{net} underestimation of 20 W/m^2 is caused by the albedo overestimation of 26%. In addition, Figure 18 shows that the net infrared is also closer to observations. It is expected that the net radiation is better represented in the combined sensitivity experiment, which is confirmed when looking at Figure 19. The R_{net} overestimation is reduced by about 40 W/m^2 at Agoufou before the monsoon. However, the SW_{net} underestimation from November to December is responsible for a R_{net} underestimation at Bamba and Agoufou. As discussed in section 5.1, the R_{net} dry season biases over Sahel are strongly related to the sensible heat flux biases, which is confirmed in Figure 19.

Despite nudging, the model displays some internal variability, which is documented here with the 12-member ensemble introduced above and shown as blue lines in Figures 13–17. In particular, the analysis of the albedo evolution at Wankama in these simulations shows a large dispersion (Figure 17). In some simulations, the surface albedo at Wankama is close to observations whereas in other simulations its seasonality is phase-shifted. This strong variability appears to be associated with a chaotic and competitive behavior of two types of grass in the model. This variability is probably overestimated and further analysis of the behavior is beyond the scope of this paper. The dispersion in the simulation of albedo is responsible for the internal variability in SW_{net} and R_{net} from May to June. However, Figures 16–19 also show that the inter-simulation variability is weak outside of the rainy season. The ensemble also illustrates the rapid adjustment under nudging, the inter-model dispersion being a bit larger during the first 10 days in January.

6. Conclusion

The nudging technique allows for a direct comparison of the surface energy budget simulated by a GCM with station data in West Africa.

Nudging horizontal winds toward reanalysis not only corrects the monsoon circulation over West Africa but also the simulated rainfall in relation with a better representation of the moisture flux. By correcting the major rainfall (dry) bias over Sahel, nudging allows for a comparison between model and observations for a similar climate regime without any ad hoc correction or sampling. By constraining the day-to-day variability of the local meteorology, nudging allows for the comparison between model and observations on a daily basis without requiring statistics that are otherwise needed when comparing observations with simulations performed in free climate mode. The comparison can be made directly between the mean grid cell value and local observations for some variables such as water vapor or downward energy radiative fluxes. When looking at surface reflection of solar radiation, at surface thermal emission or at turbulent fluxes however, the observational sampling of surface conditions on which those variables depend must be consistent with the specified distribution of model subgrid scale properties within the corresponding grid cell. Representativeness errors appear not to be as strong an issue as could have been first anticipated given the rather homogeneous characteristics of the Sahel landscapes and the careful choice of observational setups deployed for AMMA.

As expected, the nudging technique removes most of the chaotic nature of the model trajectory. Some randomness or sensitivity to initial conditions remains however when considering the day-to-day variation of convection and rainfall. At some particular locations, this chaotic behavior coupled to non-linearities of the scheme that drives the LAI growth during the rainy season results in tipping points in the representation of the albedo and surface radiative fluxes. It appears that such a behavior has already been identified for grass land plant functional type (Orchidee group private communication).

The nudging technique also allows for some freedom in the model, which is still sensitive to the model physical parameterizations, making it possible to explore the origins of the large energy biases that persist

in climate models. By comparing the outputs of a series of control and sensitivity experiments to site measurements, several conclusions have been reached concerning the model physics.

First the thermal plume model was identified to optimize the representation of near surface specific humidity throughout the West African region. It is important to note that this improvement due to the activation of the thermal plume model would not have been identified without nudging. Indeed in the free simulations, the old physics represents the near surface humidity on average better due to two compensating errors: an underestimated moistening by horizontal advection of moist air from the Gulf of Guinea and an underestimation of surface drying by mixing of surface air with dry free tropospheric air.

Using this improved physics, remaining biases in the representation of the energy budget and the key processes that may be at the origin of these biases have been identified. The biases and involved processes are different between the monsoon rainy season and the dry season. During the monsoon, the water cycle plays a first order control on the energetics. Because of this, the correction of moisture advection by nudging is very important in particular for the partition of net radiation between latent and sensible turbulent fluxes, and for the representation of the shadowing of solar radiation by clouds associated with convection. Conversely during the dry season, nudging does not correct much the seasonal evolution of the energy fluxes. The remaining errors are large, with order of magnitudes typical of AMIP simulations of the CMIP5 ensemble (Roehrig et al., 2013). Surprisingly, the standard version of LMDZ exhibits both a cold bias and an overestimation of the incoming solar radiation over Sahel. The solar radiation bias is due to a possible underestimation of aerosols or clouds. The cold bias is mainly a nocturnal bias and is controlled by soil thermal inertia, turbulence (in the stable boundary layer), and greenhouse effect. A larger thermal inertia would help reconcile the observed and simulated near surface temperature, but the value needed is more typical of a water saturated soil, making this explanation hardly plausible. Increasing nocturnal turbulence also improves the representation of the near-surface temperature. Increasing a minimum threshold for the mixing length to reduce nocturnal decoupling is not enough to fully reconcile model and observation. The exploration of other possible sources for the erroneous representation of the nocturnal turbulence would probably deserve further work. Finally, by favoring the persistence of high clouds over the region (by decreasing the ice crystal fall velocity), not only is the mean nocturnal temperature warmer, but the LW radiation also shows more day-to-day variability, in better agreement with observations.

Interestingly, the model with the STD physics is able to explain peaks associated with minimum values in the incoming SW radiation. Those peaks are clearly associated with mid-level clouds occurring at least once per month outside of the rainy season. Those clouds were underestimated in the OLD physics.

In this study we investigated how, for an imposed large-scale circulation, the physical processes are represented in the model, and how they control the energy budget over the region. For the dry season, since the nudged and free simulations are close to each other, it can be expected that improvements inspired from a comparison of nudged simulations and observations could in fact result in direct improvement of the climate simulations. For the rainy season however, the methodology does not help understand nor correct a priori the southward shift of the monsoon key elements in the LMDZ FREE simulations. Improvements in the nudged simulations may even result in an increase of this southward shift. However, even in this case, it should be desirable to improve the simulations in nudged rather than in free mode in order to avoid improving the position of the ITCZ thanks to error compensation.

As a complementary approach, we are also studying the “ nudging tendencies ” which measure the “ will ” of the model to depart from the real evolution of the large-scale circulation, in order to identify key elements in the parameterized physics which may explain this shift. The first results are promising although not straightforward. The large-scale biases involve all the scales from that of the physical parameterizations to that of the energy contrasts that drive the monsoon circulation, from the equatorial ocean to the Sahara. This methodology will hopefully allow for a disentanglement of the various contributions and help make progress in climate modeling of the monsoon system over West Africa.

Acknowledgments

In situ data were provided by the African Monsoon Multidisciplinary Analysis-Coupling the Tropical Atmosphere and the Hydrological Cycle (AMMA-CATCH) observatory (<http://www.amma-catch.org/>). We thank the AMMA-CATCH observatory and the station PIs Frank Timouk, Manuela Grippa, Bernard Cappelaere, Jérémie Demarty, Sylvie Galle, Jean-Martial Cohard and their staff for collecting data in a harsh environment. Most of the observations used are available through the AMMA database (<http://bd.amma-catch.org/amma-catch2/main.jsf>). The outputs of the LMDZ simulations used in this paper are available at <https://vesg.ipsl.upmc.fr/thredds/fileServer/IPSLFS/fabric/lmdz/AMMA/SimusDiallo2017/index.html>. We thank ambassador and the Minister of Higher Education and scientific research of Ivory Coast for the partial financial support of the Binta Diallo PhD. This work is part of the ACASIS project (ANR-13-SENV-0007, 2014–2018; <https://acasis.locean-ipsl.upmc.fr/>) and benefited as well from support of the CONVERGENCE (N°ANR-13-MONU-0008) and “Labex L-IPSL” projects, funded by the French National Research Agency.

References

- Ait-Mesbah, S., Dufresne, J. L., Cheruy, F., & Hourdin, F. (2015). The role of thermal inertia in the representation of mean and diurnal range of surface temperature in semiarid and arid regions. *Geophysical Research Letters*, *42*, 7572–7580. <https://doi.org/10.1002/2015GL065553>.

- Bateni, S. M., Entekhabi, D., Margulis, S., Castellì, F., & Kergoat, L. (2014). Coupled estimation of surface heat fluxes and vegetation dynamics from remotely sensed land surface temperature and fraction of photosynthetically active radiation. *Water Resources Research*, *50*, 8420–8440. <https://doi.org/10.1002/2013WR014573>
- Betts, A. K. (2004). Understanding hydrometeorology using global models. *Bulletin of American Meteorological Society*, *85*, 1673–1688. <https://doi.org/10.1175/BAMS-85-11-1673>
- Blackadar, A. K. (1962). The vertical distribution of wind and turbulent exchange in neutral atmosphere. *Journal of Geophysical Research*, *67*, 3095–3102.
- Bony, S., & Emanuel, K. A. (2001). A parameterization of the cloudiness associated with cumulus convection; evaluation using TOGA COARE data. *Journal of Atmospheric Sciences*, *58*, 3158–3183.
- Bosveld, F. C., Baas, P., Steeneveld, G.-J., Holtslag, A. A. M., Angevine, W. M., Bazile, E., . . . Svensson, G. (2014). The Third GABLS intercomparison case for evaluation studies of boundary-layer models. Part B: Results and process understanding. *Boundary-Layer Meteorology*, *152*, 157–187. <https://doi.org/10.1007/s10546-014-9919-1>
- Boulain, N., Cappelaere, B., Ramier, D., Issoufou, H. B. A., Halilou, O., Seghier, J., . . . Timouk, F. (2009). Towards an understanding of coupled physical and biological processes in the cultivated Sahel - 2. Vegetation and carbon dynamics. *Journal of Hydrology*, *375*, 190–203. <https://doi.org/10.1016/j.jhydrol.2008.11.045>
- Bouniol, D., Couvreur, F., Kamsu-Tamo, P.-H., Leplay, M., Guichard, F., Favot, F., & O'connor, E. J. (2012). Diurnal and seasonal cycles of cloud occurrences, types, and radiative impact over West Africa. *Journal of Applied Meteorology and Climatology*, *51*, 534–553. <https://doi.org/10.1175/JAMC-D-11-051.1>
- Cescatti, A., Marcolla, B., Vannan, S. K. S., Pan, J. Y., Román, M. O., Yang, X., . . . Migliavacca, (2012). Intercomparison of MODIS albedo retrievals and in situ measurements across the global FLUXNET network. *Remote Sensing of Environment*, *121*, 323–334.
- Charney, J. G. (1975). Dynamics of deserts and drought in the Sahel. *Quarterly Journal of the Royal Meteorological Society*, *101*, 193–202. <https://doi.org/10.1002/qj.49710142802>
- Cheruy, F., Campoy, A., Dupont, J.-C., Ducharme, A., Hourdin, F., Haeffelin, M., . . . Idelkadi, A. (2013). Combined influence of atmospheric physics and soil hydrology on the simulated meteorology at the SIRTA atmospheric observatory. *Climate Dynamics*, *40*, 2251–2269. <https://doi.org/10.1007/s00382-012-1469-y>
- Coindreau, O., Hourdin, F., Haeffelin, M., Mathieu, A., & Rio, C. (2007). Assessment of physical parameterizations using a global climate model with stretchable grid and nudging. *Monthly Weather Review*, *135*, 1474–1489. <https://doi.org/10.1175/MWR3338.1>
- Deardorff, J. W. (1970). Preliminary results from numerical integrations of the unstable planetary boundary layer. *Journal of Atmospheric Sciences*, *27*, 1209–1211.
- Dee, D. P., Uppala, S. M., Simmons, A. J., Berrisford, P., Poli, P., Kobayashi, S., . . . Vitart, F. (2011). The ERA-Interim reanalysis: Configuration and performance of the data assimilation system. *Quarterly Journal of the Royal Meteorological Society*, *137*, 553–597. <https://doi.org/10.1002/qj.828>
- Ducharme, A., & Laval, K. (2000). Influence of the Realistic Description of Soil Water-Holding Capacity on the Global Water Cycle in a GCM. *Journal of Climate*, *13*, 4393–4413. [https://doi.org/10.1175/1520-0442\(2000\)013<4393:OTRDO>2.0.CO;2](https://doi.org/10.1175/1520-0442(2000)013<4393:OTRDO>2.0.CO;2)
- Dufresne, J.-L., Foujols, M.-A., Denvil, S., Caubel, A., Marti, O., Aumont, O., . . . Vuichard, N. (2013). Climate change projections using the IPSL-CM5 Earth System Model: From CMIP3 to CMIP5. *Climate Dynamics*, *40*, 2123–2165. <https://doi.org/10.1007/s00382-012-1636-1>
- Eltahir, E. A. B., & Gong, C. (1996). Dynamics of wet and dry years in West Africa. *Journal of Climate*, *9*, 1030–1042.
- Emanuel, K. A., & Zivkovic-Rothman, M. (1999). Development and evaluation of a convection scheme for use in climate models. *Journal of Atmospheric Sciences*, *56*, 1766–1782. [https://doi.org/10.1175/1520-0469\(1999\)056<1766:DAEOAC>2.0.CO;2](https://doi.org/10.1175/1520-0469(1999)056<1766:DAEOAC>2.0.CO;2)
- Fouquart, Y., & Bonnel, B. (1980). Computations of solar heating of the Earth's atmosphere: A new parametrization. *Contributions to Atmospheric Physics*, *53*, 35–62.
- Gaetani, M., Flamant, C., Bastin, S., Janicot, S., Lavaysse, C., Hourdin, F., . . . Bony, S. (2016). West African monsoon dynamics and precipitation: The competition between global SST warming and CO₂ increase in CMIP5 idealized simulations. *Climate Dynamics*, *48*, 1353–1373. <https://doi.org/10.1007/s00382-016-3146-z>
- Giannini, A., Saravanan, X., & Chang, X. (2002). Ocean forcing of Sahel rainfall on interannual to interdecadal time-scales. *Science*, *302*, 1027–1030.
- Grandpeix, J., Lafore, J., & Cheruy, F. (2010). A density current parameterization coupled with Emanuel's Convection Scheme. Part II: 1D simulations. *Journal of Atmospheric Sciences*, *67*, 898–922. <https://doi.org/10.1175/2009JAS3045.1>
- Grandpeix, J. Y., Phillips, V., & Tailleux, R. (2004). Improved mixing representation in Emanuel's convection scheme. *Quarterly Journal of the Royal Meteorological Society*, *130*, 3207–3222.
- Grippa, M., Kergoat, L., Boone, A., Peugeot, C., Demarty, J., Cappelaere, B., . . . the ALMIP2 working group (2016). Modelling surface runoff and water fluxes over contrasted soils in pastoral Sahel: Evaluation of the ALMIP2 land surface models over the Gourma region in Mali. *Journal of Hydrology*, *18*, 1847–1866.
- Guichard, F., Kergoat, L., Hourdin, F., Authaud, C. L., Barbier, J., Mougou, E., & Diarra, B. (2015). Le réchauffement climatique observé depuis 1950 au Sahel. IRD Editions.
- Guichard, F., Kergoat, L., Mougou, E., Timouk, F., Baup, F., Hiernaux, P., & Lavenu, F. (2009). Surface thermodynamics and radiative budget in the Sahelian Gourma: Seasonal and diurnal cycles. *Journal of Hydrology*, *375*, 161–177. <https://doi.org/10.1016/j.jhydrol.2008.09.007>
- Heysmsfield, A. J., & Donner, L. J. (1990). A scheme for parameterizing ice-cloud water content in general circulation models. *Journal of Atmospheric Sciences*, *47*, 1865–1877. [https://doi.org/10.1175/1520-0469\(1990\)047<1865:ASFPIC>2.0.CO;2](https://doi.org/10.1175/1520-0469(1990)047<1865:ASFPIC>2.0.CO;2)
- Heysmsfield, A. J., van Zadelhoff, G.-J., Donovan, D. P., Fabry, F., Hogan, R. J., & Illingworth, A. J. (2007). Refinements to ice particle mass dimensional and terminal velocity relationships for ice clouds. Part II: Evaluation and parameterizations of ensemble ice particle sedimentation velocities. *Journal of Atmospheric Sciences*, *64*, 1068. <https://doi.org/10.1175/JAS3900.1>
- Hourdin, F., Couvreur, F., & Menut, L. (2002). Parameterisation of the dry convective boundary layer based on a mass flux representation of thermals. *Journal of Atmospheric Sciences*, *59*, 1105–1123.
- Hourdin, F., Foujols, M.-A., Codron, F., Guemas, V., Dufresne, J.-L., Bony, S., . . . Bopp, L. (2013b). Impact of the LMDZ atmospheric grid configuration on the climate and sensitivity of the IPSL-CM5A coupled model. *Climate Dynamics*, *40*, 2167–2192. <https://doi.org/10.1007/s00382-012-1411-3>
- Hourdin, F., Grandpeix, J.-Y., Rio, C., Bony, S., Jam, A., Cheruy, F., . . . Roehrig, R. (2013a). LMDZ5B: The atmospheric component of the IPSL climate model with revisited parameterizations for clouds and convection. *Climate Dynamics*, *40*, 2193–2222. <https://doi.org/10.1007/s00382-012-1343-y>
- Hourdin, F., Mauritsen, T., Gettelman, A., Golaz, J.-C., Balaji, V., Duan, Q., . . . Williamson, D. (2017). The Art and Science of Climate Model Tuning. *Bulletin of the American Meteorological Society*, *98*, 589–602. <https://doi.org/10.1175/BAMS-D-15-00135.1>

- Hourdin, F., Musat, I., Guichard, F., Ruti, P. M., Favot, F., Filiberti, M., . . . Gallée, H. (2010). AMMA-model intercomparison project. *Bulletin of the American Meteorological Society*, 91, 95. <https://doi.org/10.1175/2009BAMS2791.1>
- Idelkadi, A., LeVan, P., & Hourdin, F. (2005). *A global climate model with stretchable grid and nudging: I. Simulation of tracer transport at continental scales* (Tech. Rep.). IPSL, Pôle modélisation.
- Jam, A., Hourdin, F., Rio, C., & Couvreux, F. (2013). Resolved versus parametrized boundary-layer plumes. Part III: Derivation of a statistical scheme for cumulus clouds. *Boundary-Layer Meteorology*, 147, 421–441. <https://doi.org/10.1007/s10546-012-9789-3>
- Janicot, S., Thorncroft, C. D., Ali, A., Asencio, N., Berry, G., Bock, O., . . . Acad Forecasters Team (2008). Large-scale overview of the summer monsoon over West Africa during the AMMA field experiment in 2006. *Annales Geophysicae*, 26, 2569–2595. <https://doi.org/10.5194/angeo-26-2569-2008>
- Krinner, G., Viovy, N., de Noblet-Ducoudré, N., Ogée, J., Polcher, J., Friedlingstein, P., . . . Prentice, I. C. (2005). A dynamic global vegetation model for studies of the coupled atmosphere-biosphere system. *Global Biogeochemical Cycles*, 19, GB1015. <https://doi.org/10.1029/2003GB002199>
- Leauthaud, C., Cappelaere, B., Demarty, J., Guichard, F., Velluet, C., Kergoat, L., . . . Sultan, B. (2017). A 60-year reconstructed high-resolution local meteorological data set in Central Sahel (1950–2009): Evaluation, analysis and application to land surface modelling. *EGU General Assembly Conference Abstracts*, 19, 11952.
- Lebel, T., Cappelaere, B., Galle, S., Hanan, N., Kergoat, L., Levis, S., . . . Seguis, L. (2009). AMMA-CATCH studies in the Sahelian region of West-Africa: An overview. *Journal of Hydrology*, 375, 3–13. <https://doi.org/10.1016/j.jhydrol.2009.03.020>
- Locatelli, R., Bousquet, P., Hourdin, F., Saunois, M., Cozic, A., Couvreux, F., . . . Williams, A. G. (2015). Atmospheric transport and chemistry of trace gases in LMDZ5B: Evaluation and implications for inverse modelling. *Geoscience Model Development*, 8, 129–150. <https://doi.org/10.5194/gmd-8-129-2015>
- Lohou, F., Kergoat, L., Guichard, F., Boone, A., Cappelaere, B., Cohard, J.-M., . . . Timouk, F. (2014). Surface response to rain events throughout the West African monsoon. *Atmospheric Chemistry & Physics*, 14, 3883–3898. <https://doi.org/10.5194/acp-14-3883-2014>
- Lott, F., & Miller, M. (1997). A new sub-grid scale orographic drag parametrization: Its formulation and testing. *Quarterly Journal of the Royal Meteorological Society*, 123, 101–128.
- Mamadou, O., Cohard, J. M., Galle, S., Awanou, C. N., Diedhiou, A., Kounouhewa, B., & Peugeot, C. (2014). Energy fluxes and surface characteristics over a cultivated area in Benin: Daily and seasonal dynamics. *Hydrology and Earth System Sciences*, 18, 893–914. <https://doi.org/10.5194/hess-18-893-2014>
- Morcrette, J. (1991). Radiation and cloud radiative properties in the European Centre for Medium Range Weather Forecasts forecasting system. *Journal of Geophysical Research*, 96, 9121–9132.
- Mougin, E., Demarez, V., Diawara, M., Hiernaux, P., Soumaguel, N., & Berg, A. (2014). Estimation of LAI, fAPAR and fCover of Sahel rangelands (Gourma, Mali). *Agricultural and Forest Meteorology*, 198, 155–167. <https://doi.org/10.1016/j.agrformet.2014.08.006>
- Murray, T., & Verhoef, A. (2007). Moving towards a more mechanistic approach in the determination of soil heat flux from remote measurements. *Agricultural and Forest Meteorology*, 147, 88–97. <https://doi.org/10.1016/j.agrformet.2007.06.009>
- Ramier, D., Boulain, N., Cappelaere, B., Timouk, F., Rabanit, M., Lloyd, C. R., . . . Wawrzyniak, V. (2009). Towards an understanding of coupled physical and biological processes in the cultivated Sahel - 1. Energy and water. *Journal of Hydrology*, 375, 204–216. <https://doi.org/10.1016/j.jhydrol.2008.12.002>
- Redelsperger, J.-L., Thorncroft, C. D., Diedhiou, A., Lebel, T., Parker, D. J., & Polcher, J. (2006). African Monsoon Multidisciplinary Analysis: An International Research Project and Field Campaign. *Bulletin of the American Meteorological Society*, 87(12), 1739.87. <https://doi.org/10.1175/BAMS-87-12-1739>
- Rio, C., Grandpeix, J.-Y., Hourdin, F., Guichard, F., Couvreux, F., Lafore, J.-P., . . . Idelkadi, A. (2013). Control of deep convection by sub-cloud lifting processes: The ALP closure in the LMDZ5B general circulation model. *Climate Dynamics*, 40, 2271–2292. <https://doi.org/10.1007/s00382-012-1506-x>
- Rio, C., & Hourdin, F. (2008). A thermal plume model for the convective boundary layer: Representation of cumulus clouds. *Journal of Atmospheric Sciences*, 65, 407–425.
- Rio, C., Hourdin, F., Couvreux, F., & Jam, A. (2010). Resolved versus parametrized boundary-layer plumes. Part II: Continuous formulations of mixing rates for mass-flux schemes. *Boundary-Layer Meteorology*, 135, 469–483. <https://doi.org/10.1007/s10546-010-9478-z>
- Rio, C., Hourdin, F., Grandpeix, J., & Lafore, J. (2009). Shifting the diurnal cycle of parameterized deep convection over land. *Geophysical Research Letters*, 36, L07809. <https://doi.org/10.1029/2008GL036779>
- Roehrig, R., Bouniol, D., Guichard, F., Hourdin, F., & Redelsperger, J.-L. (2013). The present and future of the west african monsoon: A process-oriented assessment of cmip5 simulations along the amma transect. *Climate Dynamics*, 26, 6471–6505. <https://doi.org/https://doi.org/10.1175/JCLI-D-12-00505.1>
- Sadourny, R., & Laval, K. (1984). January and July performance of the LMD General Circulation Model, *New Perspectives in Climate Modelling*, 13, 173–198.
- Samain, O., Kergoat, L., Hiernaux, H., Guichard, F., Mougin, E., Timouk, F., & Lavenu, F. (2008). Analysis of the in situ and modis albedo variability at multiple time-scales in the Sahel. *Journal of Geophysical Research*, 113, D14119. <https://doi.org/10.1029/2007JD009174>
- Sandu, I., Beljaars, A., Bechtold, P., Mauritsen, T., & Balsamo, G. (2013). Why is it so difficult to represent stably stratified conditions in numerical weather prediction (NWP) models? *Journal of Advances in Modeling Earth Systems*, 5, 117–133. <https://doi.org/10.1002/jame.20013>
- Schmitt, C. G., & Heymsfield, A. J. (2009). The Size Distribution and Mass-Weighted Terminal Velocity of Low-Latitude Tropopause Cirrus Crystal Populations. *Journal of Atmospheric Sciences*, 66, 2013–2028. <https://doi.org/10.1175/2009JAS3004.1>
- Settle, J. J., Bharmal, N. A., Robinson, G. J., & Slingo, A. (2008). Sampling uncertainties in surface radiation budget calculations in RADAGAST. *Journal of Geophysical Research*, 113, D00E02. <https://doi.org/10.1029/2008JD010509>
- Slingo, A., White, H. E., Bharmal, N. A., & Robinson, G. J. (2009). Overview of observations from the RADAGAST experiment in Niamey, Niger: 2. Radiative fluxes and divergences. *Journal of Geophysical Research*, 114, D00E04. <https://doi.org/10.1029/2008JD010497>
- Stocker, T., Qin, G.-K. D., Plattner, M., Tignor, S., Allen, J., Boschung, A., . . . Midgley, P. (Eds.) (2013). *IPCC, 2013: Climate change 2013: The physical science basis. Contribution of working group I to the fifth assessment report of the intergovernmental panel on climate change* (1535 pp.). Cambridge, UK: Cambridge University Press. <https://doi.org/10.1017/CBO9781107415324>
- Taylor, C. M., Gounou, A., Guichard, F., Harris, P. P., Ellis, R. J., Couvreux, F., & de Kauwe, M. (2011). Frequency of Sahelian storm initiation enhanced over mesoscale soil-moisture patterns. *Nature Geoscience*, 4, 430–433. <https://doi.org/10.1038/ngeo1173>
- Timouk, F., Kergoat, L., Mougin, E., Lloyd, C. R., Ceschia, E., Cohard, J.-M., . . . Taylor, C. M. (2009). Response of surface energy balance to water regime and vegetation development in a Sahelian landscape. *Journal of Hydrology*, 375, 178–189. <https://doi.org/10.1016/j.jhydrol.2009.04.022>
- Tsvetinskaya, E. A., Schaaf, C. B., Gao, F., Strahler, A. H., Dickinson, R. E., Zeng, X., & Lucht, W. (2002). Relating MODIS-derived surface albedo to soils and rock types over Northern Africa and the Arabian peninsula. *Journal of Geophysical Research*, 29(9), 1353. <https://doi.org/10.1029/2001GL014096>

- Van Weverberg, K., Vogelmann, A. M., Lin, W., Luke, E. P., Cialella, A., Minnis, P., . . . Jensen, M. P. (2013). The role of cloud microphysics parameterization in the simulation of mesoscale convective system clouds and precipitation in the tropical western Pacific. *Journal of Atmospheric Sciences*, *70*, 1104–1128. <https://doi.org/10.1175/JAS-D-12-0104.1>
- Verhoef, A., Ottlé, C., Cappelaere, B., Murray, T., Saux-Picart, S., Zribi, M., . . . Ramier, D. (2012). Spatio-temporal surface soil heat flux estimates from satellite data; results for the AMMA experiment at the Fakara (Niger) supersite. *Agricultural and Forest Meteorology*, *154*, 55–66. <https://doi.org/10.1016/j.agrformet.2011.08.003>
- Wang, F., Cheruy, F., & Dufresne, J.-L. (2016). The improvement of soil thermodynamics and its effects on land surface meteorology in the IPSL climate model. *Geoscientific Model Development*, *9*, 363–381. <https://doi.org/10.5194/gmd-9-363-2016>
- Yamada, T. (1983). Simulations of nocturnal drainage flows by a q^2l turbulence closure model. *Journal of Atmospheric Sciences*, *40*, 91–106.